NASA Contractor Report 4766

Validation of an Accurate Three-Dimensional Helical Slow-Wave Circuit Model

Carol L. Kory

CONTRACT NAS3–27600
MARCH 1997

National Aeronautics and
Space Administration

NASA Contractor Report 4766

Validation of an Accurate Three-Dimensional Helical Slow-Wave Circuit Model

Carol L. Kory
Analex Corporation
Brook Park, Ohio

Prepared for
Lewis Research Center
under Contract NAS3–27600

National Aeronautics and
Space Administration

Office of Management
Scientific and Technical
Information Program

1997

Contents

VALIDATION OF AN ACCURATE THREE-DIMENSIONAL HELICAL SLOW-WAVE CIRCUIT MODEL

Carol L. Kory

ABSTRACT

The helical slow-wave circuit embodies a helical coil of rectangular tape supported in a metal barrel by dielectric support rods. Although the helix slow-wave circuit remains the mainstay of the traveling-wave tube (TWT) industry because of its exceptionally wide bandwidth, a full helical circuit, without significant dimensional approximations, has not been successfully modeled until now. Numerous attempts have been made to analyze the helical slow-wave circuit so that the performance could be accurately predicted without actually building it, but because of its complex geometry, many geometrical approximations became necessary rendering the previous models inaccurate. In the course of this research it has been demonstrated that using the simulation code, MAFIA, the helical structure can be modeled with actual tape width and thickness, dielectric support rod geometry and materials. To demonstrate the accuracy of the MAFIA model, the cold-test parameters including dispersion, on-axis interaction impedance and attenuation have been calculated for several helical TWT slow-wave circuits with a variety of support rod geometries including rectangular and T-shaped rods, as well as various support rod materials including isotropic, anisotropic and partially metal coated dielectrics. Compared with experimentally measured results, the agreement is excellent.

With the accuracy of the MAFIA helical model validated, the code was used to investigate several conventional geometric approximations in an attempt to obtain the most computationally efficient model. Several simplifications were made to a standard model including replacing the helical tape with filaments, and replacing rectangular support rods with shapes conforming to the cylindrical coordinate system with effective permittivity. The approximate models are compared with the standard model in terms of cold-test characteristics and computational time.

The model was also used to determine the sensitivity of various circuit parameters including typical manufacturing dimensional tolerances and support rod permittivity. By varying the circuit parameters of an accurate model using MAFIA, these sensitivities can be computed for manufacturing concerns, and design optimization previous to fabrication. Thus, the need for costly experimental iterations can be eliminated. Several variations were made to a standard helical circuit using MAFIA to investigate the effect that variations on helical tape and support rod width, metallized loading height and support rod permittivity have on TWT cold-test characteristics.

I. INTRODUCTION

The traveling-wave tube (TWT) is an electron device used for amplification at microwave frequencies, possessing four major components: 1) an electron gun which produces an electron beam, 2) a slow-wave circuit which slows an RF electromagnetic wave to a speed synchronous with the electron beam, 3) a collector which collects the spent electron beam and 4) the TWT package providing cooling, beam focusing and access to the RF input and output [1]. Amplification is obtained by feeding the RF signal to be amplified into the slow-wave circuit while the electron beam is moving along the TWT axis. The slow-wave structure slows the electromagnetic wave so that it propagates near synchronism with the electron beam, resulting in interaction between the wave and the beam, and thus amplification of the RF signal. The spent electron beam is collected at the end of the tube by the collector.

A critically important step in the design of a TWT is the determination of the slow-wave circuit dispersion, on-axis interaction impedance and RF losses. A well established procedure to acquire these parameters is to actually build and cold-test (evaluation on the RF test bench without the electron beam) a model or a scale model of the circuit and to physically adjust circuit parameters until desired performance is achieved. This procedure is extremely time-consuming, very expensive and also limits freedom to examine new variations to the basic circuit. This makes the need for computational methods crucial as they can lower cost, reduce tube development time and lessen limitations on novel designs. Computer simulation has been used in the past to obtain accurate cold-test parameters for several TWT slow-wave circuits [2,3]. Although the helix slow-wave circuit remains the mainstay of the TWT industry because of its exceptionally wide bandwidth, to the author's knowledge a full helical circuit, without significant dimensional approximations, has not been successfully modeled until now.

I.1 Helix TWT Slow-Wave Circuit Modeling History

Numerous attempts have been made to analyze the helical slow-wave circuit to predict performance prior to fabrication. Initially, Pierce approximated the helix with a sheath, or a helically conducting cylindrical sheet of the same radius and pitch as the helix [4]. Sensiper improved upon this analysis by introducing a tape model which treats the helix as having a finite width but zero thickness [5]. Tien used the tape model of Sensiper to compute the interaction impedance for a helix surrounded by a homogeneous dielectric medium in [6] where he derived an impedance reduction factor relating the impedance of a tape helix surrounded by a dielectric medium to the impedance of a sheath helix in free-space. Tien replaced the support bars with a single continuous homogeneous dielectric volume with an effective permittivity. McMurtry took this analysis one step further by including the effect of a surrounding conducting shield [7]. As interest in dispersion shaping of helical circuits increased, and variously shaped dielectric support rods were employed, the dielectric supports could no longer be accurately modeled by replacing them with a homogeneous volume. Jain and Basu addressed this problem in [8] by smoothing out the dielectric rods azimuthally into a large number of dielectric tubes of their respective effective permittivity values. In the analysis of [8], a sheath helix is used in the model. Sinha et al. [9] use the same inhomogeneous loading method with a tape helix model. Even with all of these improvements to the initial analyses, the latest theoretical models still do not show good agreement compared to experimentally measured results [9].

I.2 Introduction to MAFIA

This study involves the use of MAFIA (Solution of **MA**xwell's equations by the **F**inite-**I**ntegration-**A**lgorithm), a powerful, electrodynamic code written in FORTRAN 77 that is used for computer-aided design of two-dimensional and fully three-dimensional electromagnetic devices such as magnets, RF cavities, waveguides, antennas, etc. The Finite Integration Technique (FIT) algorithm produces a matrix of finite-difference equations for electric and magnetic field vectors in the structure under study. The solution of these equations yields static, frequency-domain or time-domain solutions of Maxwell's equations [10,11]. The code

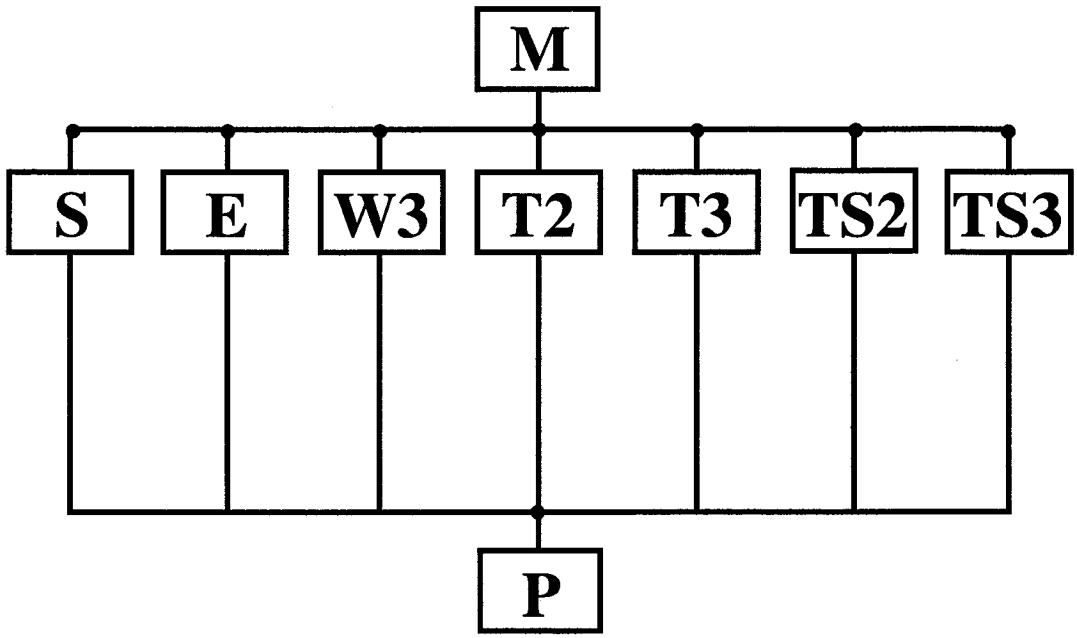

Figure 1 MAFIA organizational chart

includes nine modules which posses inter-relationships as shown in Figure 1, with each module containing several sections. The cold-test characteristics of this report were calculated using the M (mesh generator), E (eigenmode solver), and P (postprocessor) modules of MAFIA. The remaining modules are, S (static solver), T2/T3 (two-dimensional (2D) and three-dimensional (3D) time domain solvers, respectively), TS2/TS3 (2D and 3D particle-in-cell codes, respectively) and W3 (3D frequency domain solver).

I.3 Perspective

Chapter II goes through the detailed analysis of how cold-test characteristics are calculated for TWT slow-wave circuits using MAFIA. Then to demonstrate the accuracy of the MAFIA code applied specifically to helical TWT slow-wave circuits, the dispersion, on-axis interaction impedance and attenuation have been calculated for a C-Band helix TWT using MAFIA and compared to measured data [12] in Chapter III. The C-Band circuit is also used as a model to investigate conventional helical geometrical approximations from the cited literature [4, 5, 6, 7 and 8] and their effect on computational time and accuracy. Such approximations as smeared support rods and infinitesimally thin helix wire are explored.

Chapter IV reports on the results of a broadband helical circuit embodying a partial metal coating on the support rods. The metal film makes this circuit more complicated to model, as well as to fabricate. The dispersion, on-axis interaction impedance and attenuation have been calculated and are compared to experiment [12] here. In addition, several variations are performed on this circuit to obtain the sensitivity of various circuit parameters. The results include variations to the metal film radius, tape width and dielectric support rod width and permittivity.

Lastly, two other TWT slow-wave circuits are modeled using MAFIA to demonstrate the wide variety of structures which can be studied. Included are circuits with rectangular anisotropic pyrolytic boron nitride (APBN) and T-shaped BeO support rods. The results obtained using MAFIA are compared with measured data [13,14] in Chapter V. The work reported here is summarized and discussed in Chapter VI and future work involving the three-dimensional simulation of vacuum device components discussed.

II. ANALYSIS AND SIMULATION

II.1 Dispersion

The dispersion relation was calculated similar to experimental methods in which the frequency-phase dispersion characteristics are calculated by measuring the resonant frequencies in a truncated circuit section. The resonances correspond to standing waves, such that there is an integral number of half wavelengths (phase shifts of π) in the circuit length. Truncating the model with either an electric or magnetic wall with MAFIA corresponds to simulating standing waves in the length of the circuit. An electric wall is a boundary which simulates a perfect conductor with the electric field perpendicular to the wall. At a magnetic wall boundary condition the tangential magnetic field is zero and the magnetic field is perpendicular to the wall. The phase shifts per turn for the helix, obtained by modeling ten turns and truncating the model with an electric boundary condition at one axial end and a magnetic boundary condition at the other, are listed in Table I. The phase shifts per turn for the resulting resonant frequencies are listed in order of increasing frequency for the fundamental RF space harmonic (n = 0) mode. Although the helical circuit has no symmetry planes, truncating the slow-wave circuit section with these boundaries is correct on the axis and gives accurate results as long as enough turns are modeled to reduce the contributions of the fields at the end sections to an insignificant level.

II.2 On-axis Interaction Impedance

The on-axis interaction impedance is a figure of merit proportional to the strength between the RF wave and the electron beam, defined for the n^{th} RF space harmonic [15] as

$$K_n = \frac{|E_n^2|}{2\beta_n^2 P_{RF}} \tag{1}$$

where $|E_n|$ is the axial electric field magnitude of the n^{th} space harmonic and β_n is the axial phase constant of the n^{th} harmonic defined by

$$\beta_n = \frac{\phi + 2\pi n}{L} \quad . \tag{2}$$

ϕ is the phase shift per turn in radians of the fundamental harmonic, n is the space harmonic order and L is the length of one turn. P_{RF} is the time averaged RF power flow defined by

Table I Boundary conditions for resonance at various phase shifts per turn for a ten turn slow-wave structure

Number of Turns	Boundary Conditions	Phase shift per turn, βL (degrees)
10	Magnetic/Electric	9, 27, 45, 63, 81, 99, 117, 135, 153, 171

$$P_{RF} = w v_g \tag{3}$$

where v_g is the group velocity and w is the time averaged stored electromagnetic energy per unit length,

$$w = \frac{W_T}{NL} , \tag{4}$$

with W_T the total energy in the N turns.

Synchronism with the beam for the helix is desirable for the fundamental RF space harmonic thus we need to calculate the fundamental (n = 0) harmonic term in Equation 1 to determine the on-axis interaction impedance which is related to the gain of the circuit and is used as an input in various TWT modeling codes. To determine the interaction impedance of the backward wave mode as related to backward gain (backward wave oscillations) we need to calculate the n = -1 term in Equation 1.

In order to determine the magnitude, $|E_n|$, a Fourier analysis is performed (Appendix A) on the total on-axis axial electric field, E_{ztot}. The effective field as seen by the electron beam is the peak value of the particular space harmonic with which the beam is synchronous. This value of the field for a traveling wave, $|E_n|$, is half that calculated with MAFIA for a standing wave, $|E_{nS}|$ [16], so the value needed for Equation 1 is

$$|E_n| = \frac{1}{2}|E_{nS}| . \tag{5}$$

To obtain W_T for Equation 4, the #energy section of the P module of MAFIA is used to calculate the total time averaged electromagnetic field energy for a standing wave, W_S. The total energy for a traveling wave is half that calculated for a standing wave, [16] so the total energy of Equation 4 is

$$W_T = \frac{1}{2} W_S . \tag{6}$$

Therefore, the total stored electromagnetic energy per unit length for a traveling wave, w, is

$$w = \frac{1}{2}\frac{W_S}{NL} \tag{7}$$

and the total RF power flow can be defined as

$$P_{RF} = \frac{1}{2}\frac{W_S}{NL} v_g . \tag{8}$$

The group velocity of Equation 3 is defined as

$$v_g = \frac{\partial \omega}{\partial \beta_n} \tag{9}$$

and is extracted from the dispersion curve which is plotted with frequency versus $\beta_n L$ (in degrees). Using these parameters, v_g can be expressed as

$$v_g = 360 L \frac{\partial f}{\partial(\beta_n L)} . \tag{10}$$

Thus, the on-axis interaction impedance can be expressed as

$$K_n = \frac{|E_{nS}{}^2| \, NL}{4\beta_n^2 \, W_S \, v_g} \quad . \tag{11}$$

For simplicity, βL will imply $\beta_0 L$, the phase shift per turn for the n=0 space harmonic, throughout the rest of the text.

II.3 Attenuation

The circuit attenuation is calculated using the same truncation method as with the dispersion and impedance calculations. The attenuation, α, is defined in dB per unit length as

$$\alpha = 8.686 \frac{P_L}{2 P_{RF}} \tag{12}$$

[17] where P_L is the total power loss per unit length

$$P_L = \frac{P_{LT}}{NL} \tag{13}$$

and P_{LT} is the total power loss for a traveling wave in the N turns. The total RF power flow is calculated from Equation 8, and the total power loss for a standing wave is usually calculated in the #losses section. The total power loss for a traveling wave is half that calculated for a standing wave (see Appendix B)

$$P_{LT} = \frac{1}{2} P_{LS} \quad . \tag{14}$$

Therefore, the attenuation in dB per unit length can be expressed as

$$\alpha = 4.343 \frac{P_{LS}}{W_S v_g} \quad . \tag{15}$$

The attenuation in dB/turn can be expressed as

$$\alpha = 4.343 \frac{P_{LS} \, L}{W_S v_g} \quad . \tag{16}$$

The presence of dielectric supports necessitates attenuation calculations for both conductive surfaces and dielectrics. The current version of MAFIA (3.20) does not include the capability to calculate the power loss in dielectric materials in the cylindrical coordinate system. The user is faced with two options, to neglect these losses since they will be significantly less than the power loss from the conductive surfaces, or to model in the Cartesian coordinate system. Here, we have chosen to calculate the losses due to conductive surfaces with the standard model in the cylindrical coordinate system. Then we have used a simplified model in the Cartesian coordinate system, where the helical tape is replaced by filaments, to obtain the losses from the dielectric material. This simplified model is discussed in detail in Chapter III.

III. C-BAND HELICAL SLOW-WAVE CIRCUIT SIMULATIONS

The first circuit modeled is the helical slow-wave circuit from a Northrop Grumman C-Band TWT for the Microwave Power Module (MPM) [12]. The experimental circuit includes a rectangular, copper plated tungsten, helical tape supported by rectangular BeO rods inside a conducting barrel as shown for the end view in Figure 2.

The dispersion, on-axis interaction impedance and attenuation are calculated for this circuit using MAFIA and compared with measured results [12]. This circuit is also used as a model to investigate several geometrical approximations, and their effect on accuracy and computational time.

III.1 Cold-Test Characteristics

The current version of MAFIA (3.20) does not posses the capability to generate a helical structure automatically. Thus the helix was generated in the cylindrical coordinate system by varying axial and azimuthal coordinates consistent with the formula of a circular helix. A MAFIA three-dimensional plot of several turns of the helical circuit is shown in Figure 3. Because the support rods do not conform to the cylindrical coordinate system, "quasi-rectangular" rods were modeled in radial increments by reducing the rod angle with increasing radius to approximate rectangles. Figure 4 shows a blown up portion of a modeled quasi-rectangular rod. The helix itself was also incremented for the azimuthal coordinate by 20 degrees as shown in Figure 3.

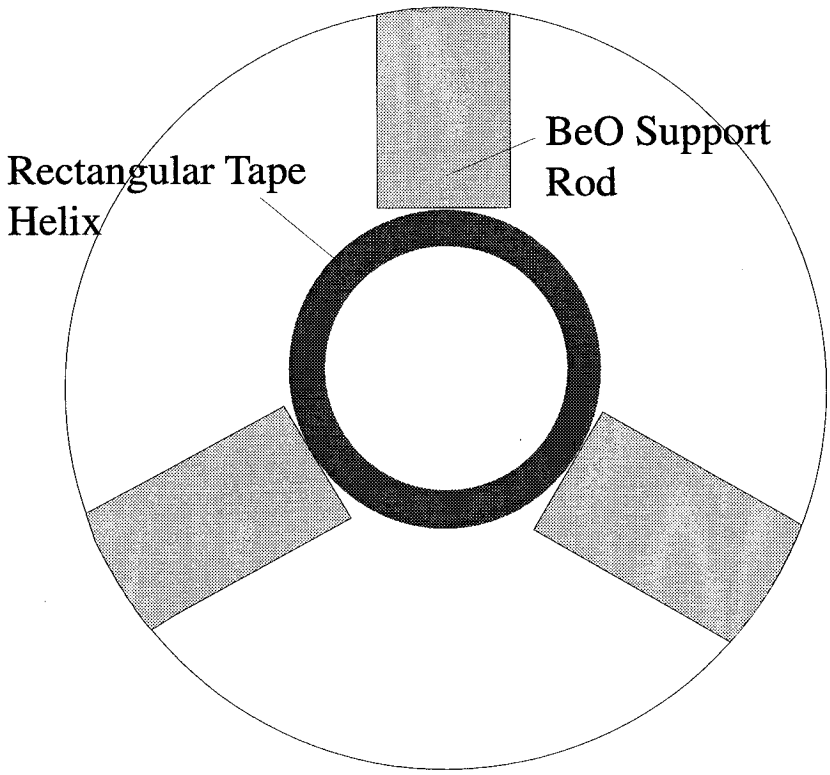

Figure 2 Northrop Grumman C-Band helical TWT slow-wave circuit

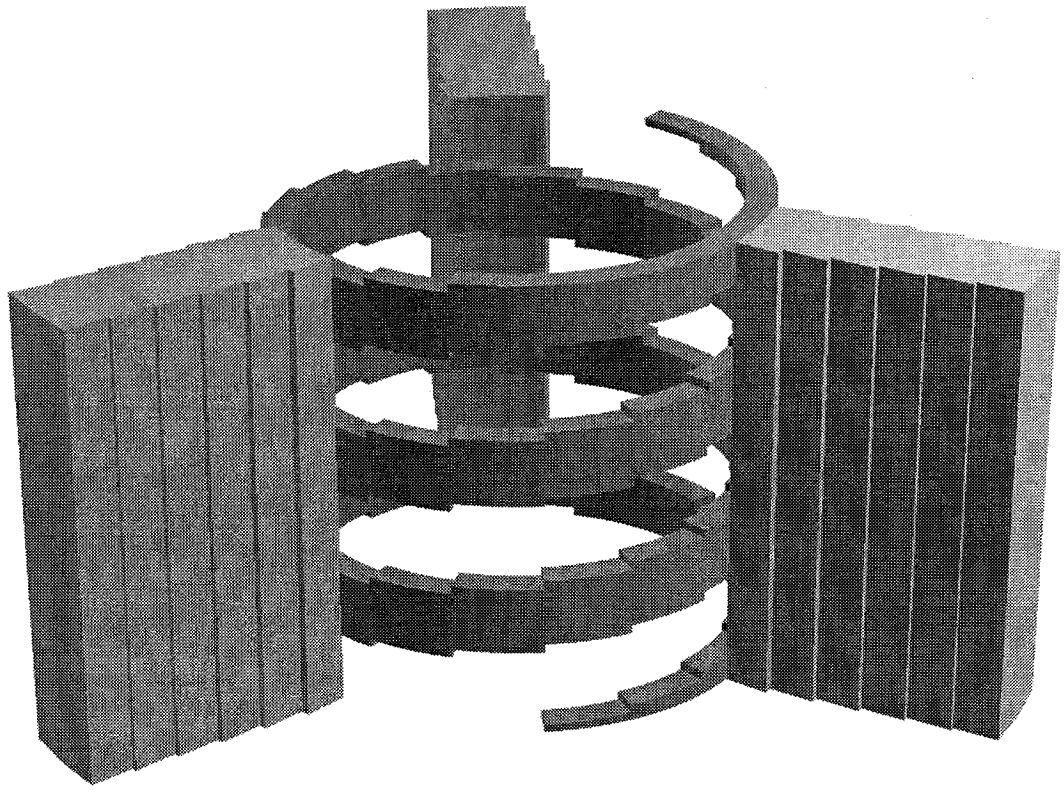

Figure 3 MAFIA three-dimensional plot of Northrop C-Band helical circuit

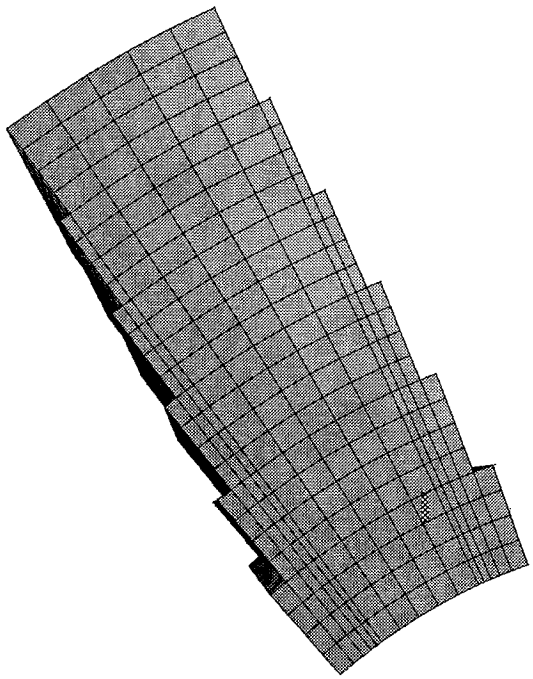

Figure 4 MAFIA blown up view of quasi-rectangular support rod for Northrop C-Band helical circuit

III.1.1 Dispersion

Using ten turns and electric and magnetic boundary conditions at either end, ten resonant frequencies at the values of βL of Table I were obtained to form the dispersion curve of Figure 5. The automatic mesh generator option was used in the #mesh section of M, the Mesh generator, using a maximum number of meshpoints equaling 150000. Thirty-five modes were requested in the #solver section of E, the Eigenmode solver. The results using MAFIA are compared to measured data for the dispersion in Figure 5 and Table II. The agreement is very good with an absolute average difference across the bandwidth of 0.71%. The modeling characteristics of Table II, including the maximum mesh points, modes requested and azimuthal increment, are used throughout this work unless otherwise specified. Table II also lists the CPU time for ten turns of the C-Band circuit using an IBM RISC/6000 Model 590 workstation.

III.1.2 On-Axis Interaction Impedance

The on-axis interaction impedance was calculated for ten points consistent with the method outlined in Chapter II. The results calculated using MAFIA are compared with measured data in Figure 6. The MAFIA results differ by an absolute average difference of about six Ohms across the bandwidth.

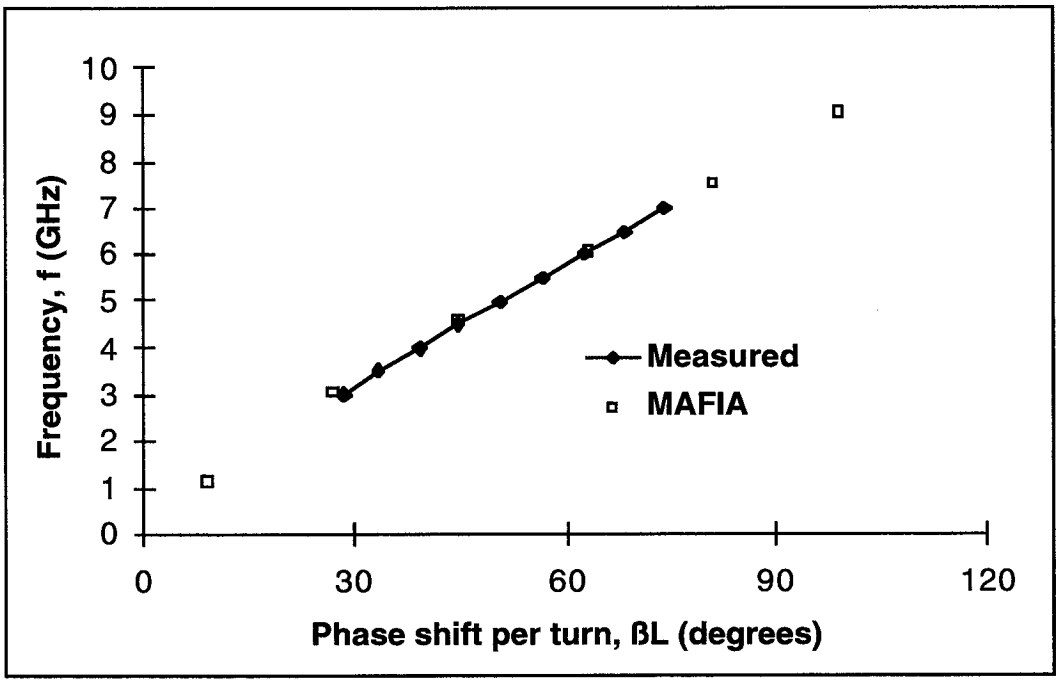

Figure 5 Measured and simulated dispersion for Northrop C-Band helical circuit

Table II Modeling information for ten turns of Northrop C-Band helical circuit (RISC/6000 Model 590 Workstation)

Maximum Mesh Points in Mesh Generator	Modes Requested in Eigenmode Solver	Helix Tape Azimuthal Increments (degrees)	Support Rod Radial Increments (Number of)	Average Absolute Frequency Difference (%)	CPU (hrs:mins)
150000	35	20	6	0.71	30:05

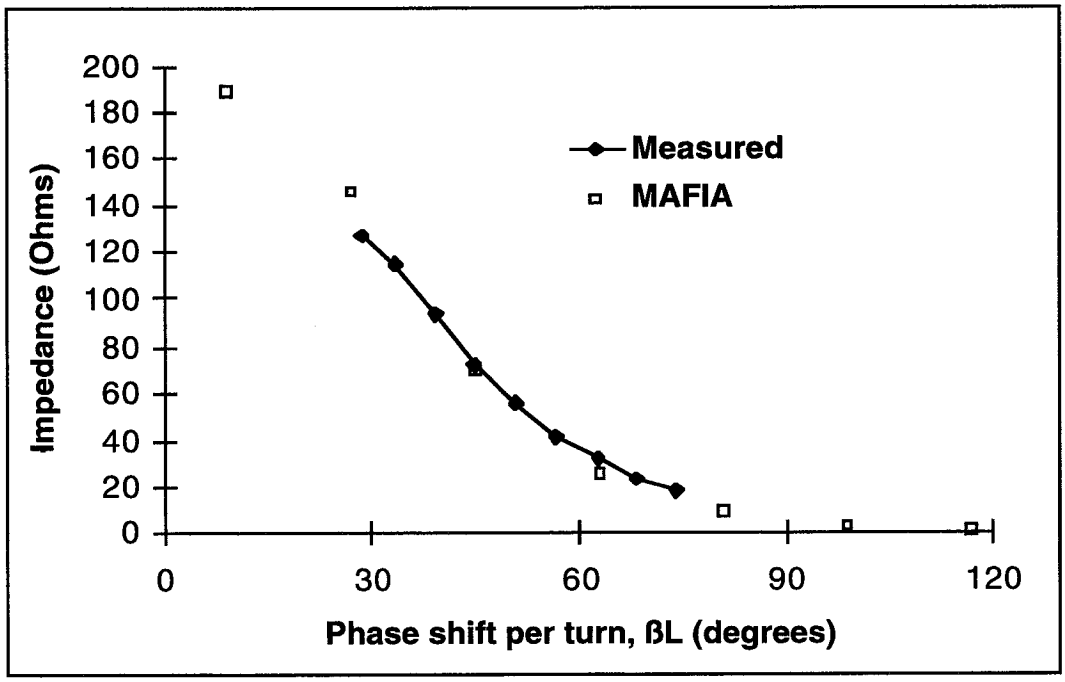

Figure 6 Measured and simulated on-axis interaction impedance for Northrop C-Band helical circuit

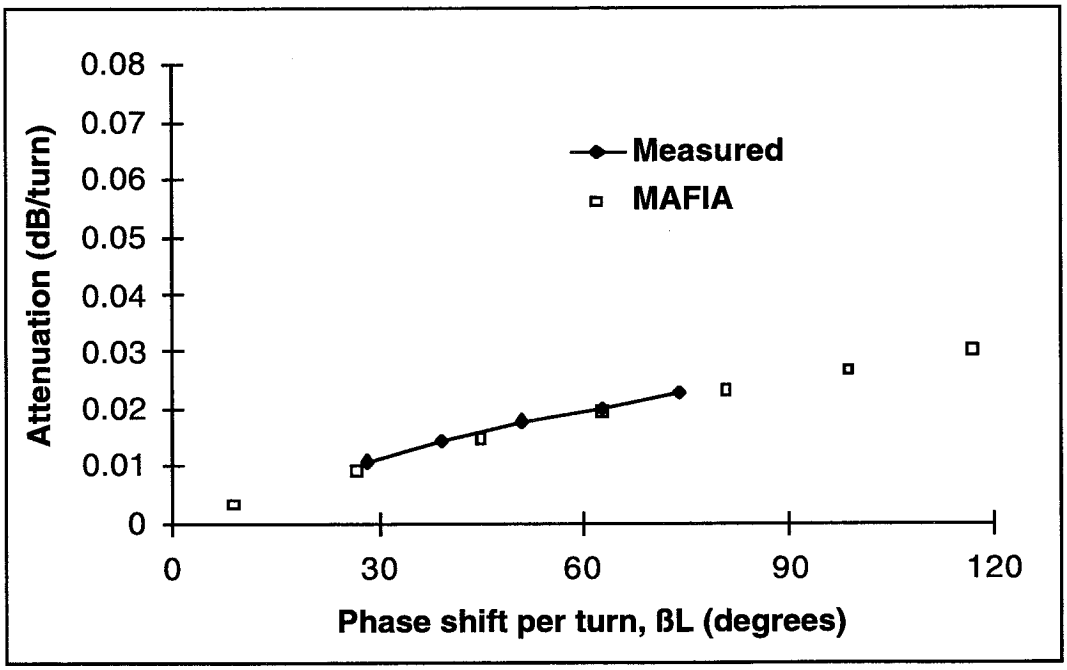

Figure 7 Measured and simulated attenuation for Northrop C-Band helical circuit

III.1.3 Attenuation

Figure 7 compares the attenuation for the MAFIA model with measured values. The necessary MAFIA input includes an effective conductivity value and appropriate dielectric loss tangent. The loss tangent for BeO was taken to be .0001. The effective conductivity value was taken from Gilmour et al. [18] where theoretical and experimental TWT helix loss was determined from about 2 to 16 GHz for a copper plated helix. Gilmour et al. found excellent agreement between calculated and measured loss when helix surface roughness was assumed to cause the resistivity to increase by a factor of approximately two. Using a conductivity consistent with these results (1.45×10^7 S/m), the average absolute attenuation difference was about .0005 dB per turn.

III.2 Examination of Conventional Geometric Approximations

To investigate the effect of applying some of the conventional geometric approximations discussed in Chapter I, the full MAFIA model was simplified in several ways and the cold-test characteristics calculated. The effect these approximations have on accuracy, relative to measured data, and CPU time were determined. First, approximations for the helical tape were investigated by replacing the tape by a series of filaments, or infinitesimally thin, perfectly conducting wires. The quasi-rectangular support rods were then replaced with several approximate models including a single uniform volume of uniform effective dielectric constant, three uniform wedges of uniform effective dielectric constant, a graded volume with graded effective dielectric constants and graded wedges with graded effective dielectric constants.

III.2.1 Helical Tape

The tape helix of the MAFIA model shown in Figure 3 was replaced with filaments, or infinitesimally thin, perfectly conducting wires in the Cartesian coordinate system. This simplified model is shown in Figure 8, where the tape helix is represented by three filaments placed at the inner, average and outer helical radii.

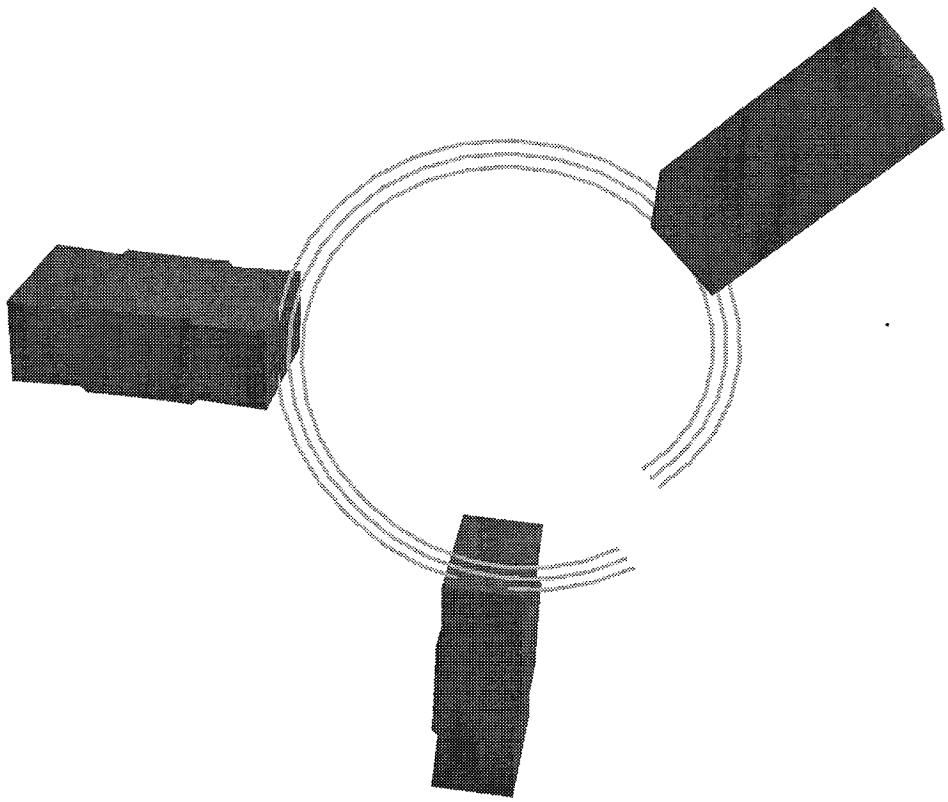

Figure 8 MAFIA three-dimensional model of one turn of Northrop C-Band helical circuit with filaments replacing tape helix

Since the filament is a perfectly conducting wire, the attenuation data for these models is incomplete, so the dispersion and on-axis interaction impedance are compared. Starting with one filament at the average helix radius (designated r1), the number of filaments was increased to seven filaments (r7) uniformly filling out the radial thickness of the helical tape. Figure 9 and Figure 10 show the dispersion and on-axis interaction impedance, respectively, for this series of simulations compared to the standard MAFIA model. It appears that both the dispersion and impedance converge with three filaments (r3). Thus, the remaining simulations will be done with three radial filaments placed at the inner, average and outer helical radii.

Next, using three filaments in the radial direction placed at the inner, average and outer helical radii, filaments were incrementally added in the axial direction to take into account the finite width of the helical tape, so the tape is "caged in". The results for the dispersion and on-axis interaction impedance converged at five axial filaments for a total number of 15 filaments representing the helical tape (designated r3z5). The dispersion and impedance for the axial series of simulations is not shown to avoid repetition. Figure 11 compares the measured and simulated dispersion for the standard, r3 and r3z5 models showing a slight improvement with the addition of the filaments in the axial direction. Using filaments resulted in a lack of convergence at various values of phase shift per turn. To help alleviate this problem, the maximum number of meshpoints was increased to 175,000 in the Mesh generator, and the number of modes requested was increased to 40 in the Eigenmode solver. It is obvious that the accuracy obtained with the filament model is not as good as that obtained with the standard model, especially at higher frequencies where the electric fields are concentrated between the helical turns, rendering the effects of this approximation more significant [19]. The on-axis interaction impedance is compared for the same models in Figure 12 showing very slight disagreement between the standard and r3z5 models. The CPU times are compared in Table III, showing a large savings in computational time with both r3 and r3z5. All things taken into consideration, r3z5 is the better of the two filament models. These results imply that filaments could be used if a quick approximate analysis is needed, especially if the data needed is at lower values of phase shift per turn, where this model provides fairly accurate results.

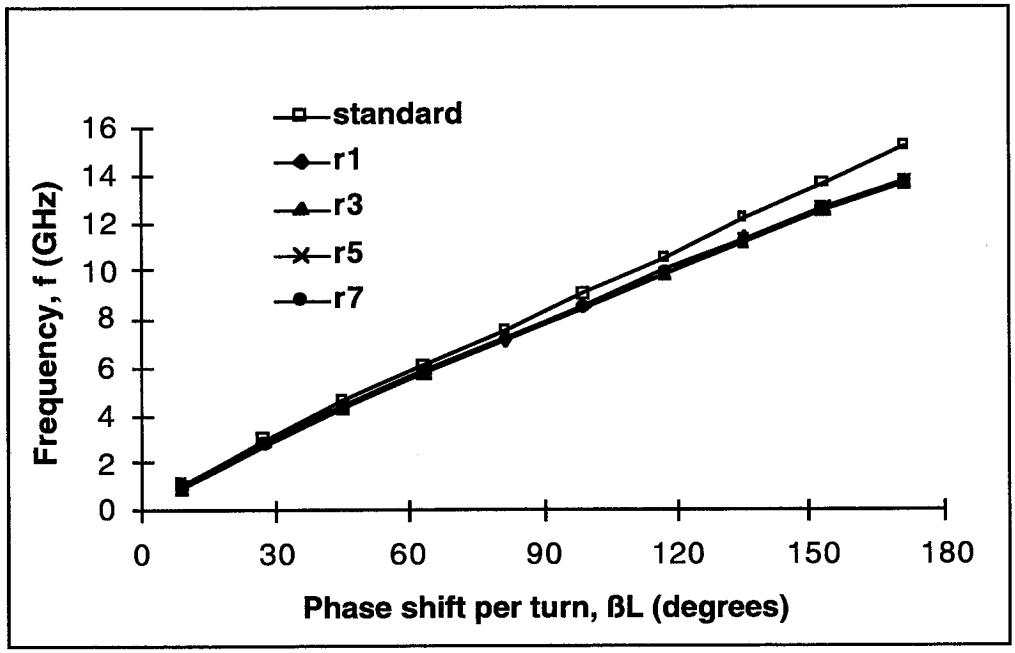

Figure 9 Simulated dispersion for Northrop C-Band helical circuit with modeled helical tape replaced by radially placed filaments

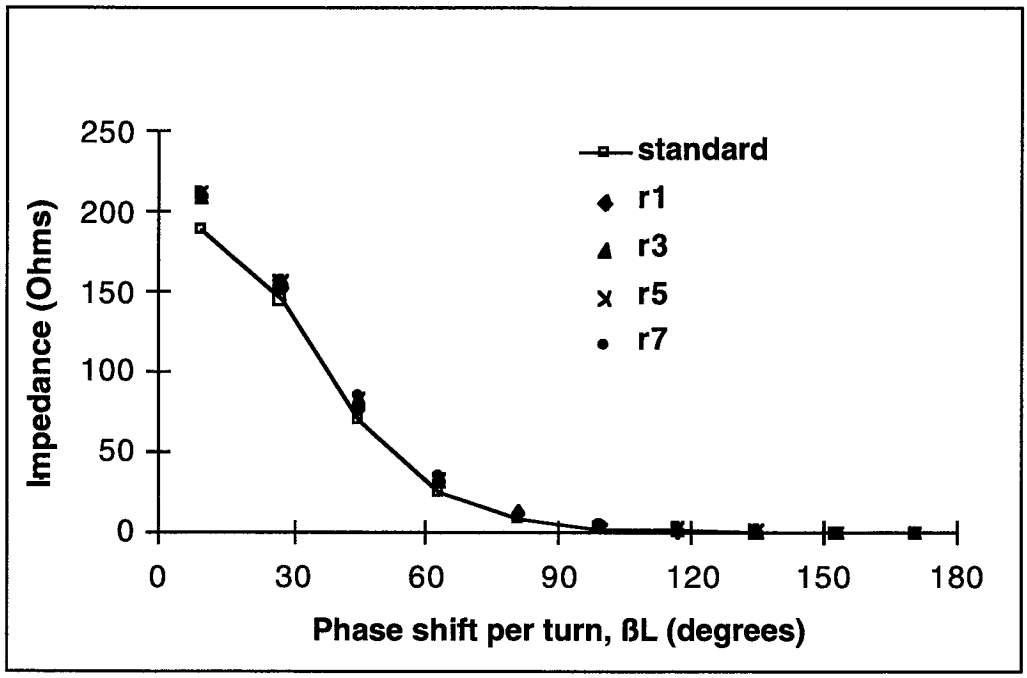

Figure 10 Simulated on-axis interaction impedance for Northrop C-Band helical circuit with modeled helical tape replaced by radially placed filaments

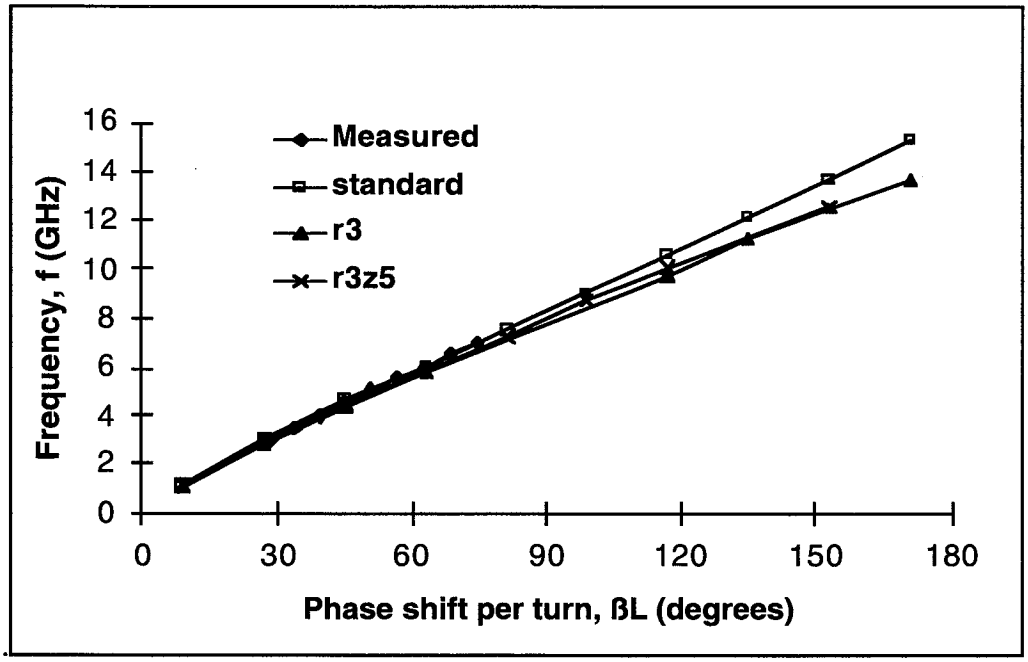

Figure 11 Measured and simulated dispersion for Northrop C-Band helical circuit comparing standard, r3 and r3z5 models

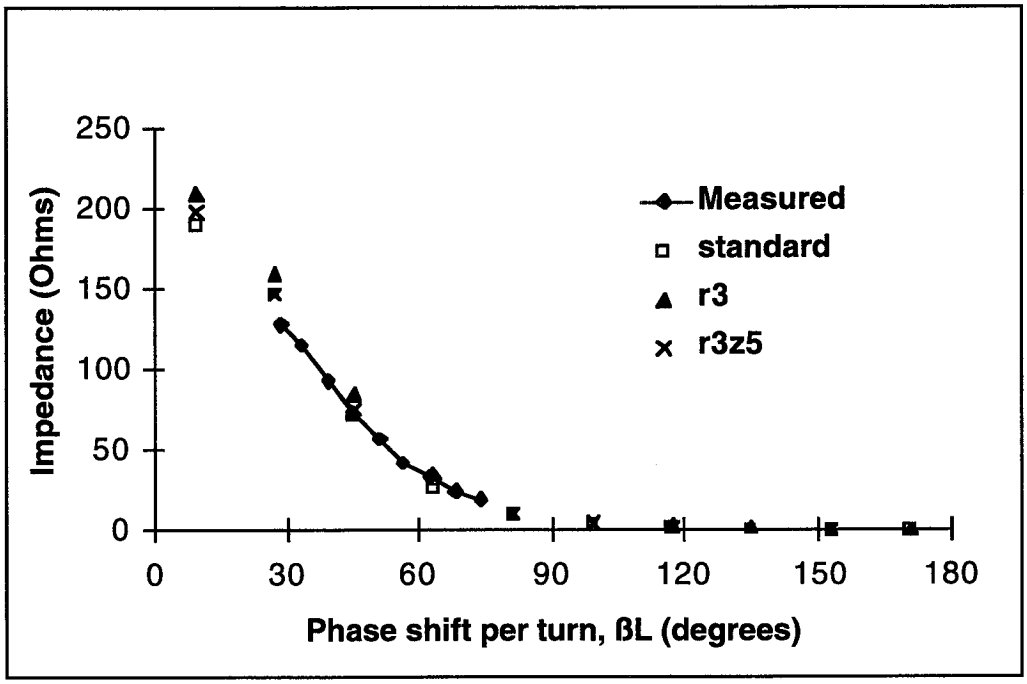

Figure 12 Measured and simulated on-axis interaction impedance for Northrop C-Band helical circuit comparing standard, r3 and r3z5 models

Table III CPU comparison for helical tape models of ten turns of the Northrop C-Band helical circuit (RISC/6000 Model 590 Workstation)

Helical Tape Model	CPU (hrs:mins)
Standard	30:05
r3	2:04
r3z5	1:59

III.2.2 Dielectric Support Rods

Several approximate models for the support rods were investigated. First the quasi-rectangular rods of the standard model were replaced by a uniform volume homogeneously filling the space between the helix and the outer barrel, with effective dielectric constant, ε_r', calculated from the relationship

$$\varepsilon_r' = 1+(\varepsilon_r - 1)\frac{A}{A'} \tag{17}$$

where ε_r' and A' are the effective dielectric constant and cross-sectional surface area, respectively, of the uniform volume in the MAFIA model. ε_r and A are the actual dielectric constant and cross-sectional surface area of the actual rectangular rods. The support rods are made of BeO, so the nominal value for ε_r would be about 6.5. The cross-sectional view of this model is shown in Figure 13. Next, uniform wedges with width consistent with the actual support rod width at the point of contact with the helix, and appropriate effective dielectric constant consistent with the cross-sectional area of the wedges and Equation 17, were used to approximate the rectangular support rods. The cross-sectional view of the uniform wedge configuration is shown in Figure 14.

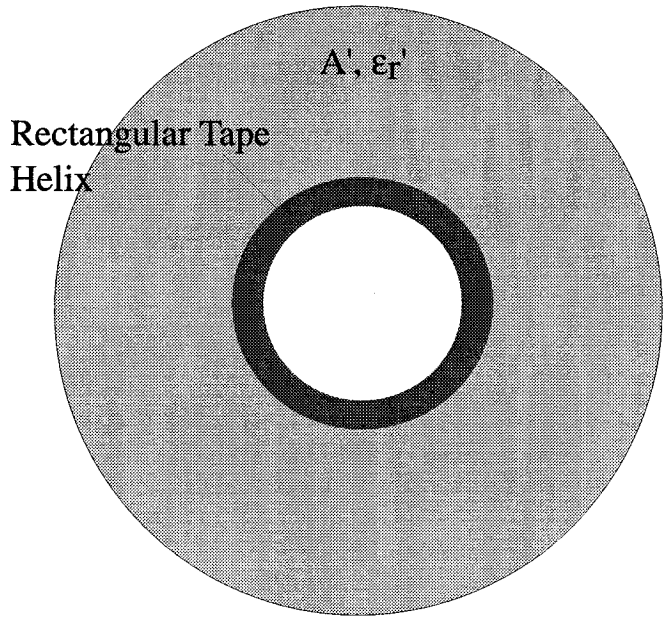

Figure 13 Northrop C-Band helical circuit uniform volume support rod model

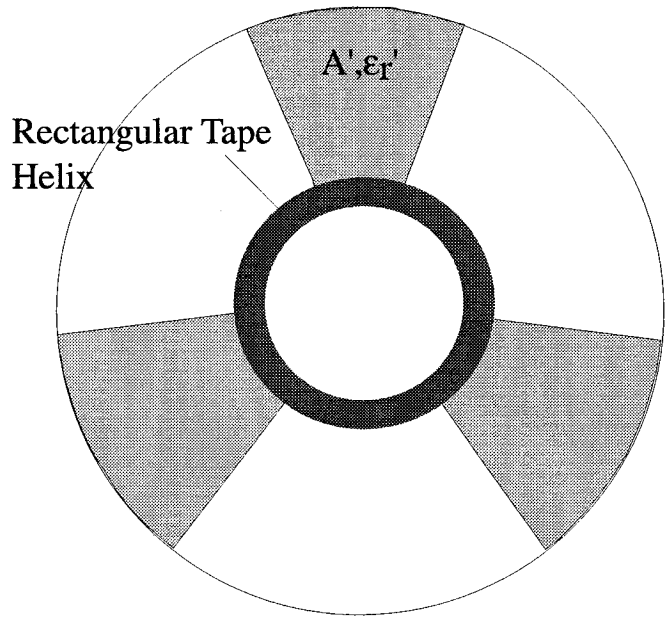

Figure 14 Northrop C-Band helical circuit uniform wedge support rod model

The dispersion is compared for each of these rod configurations to the standard quasi-rectangular rod model and measured values in Figure 15. The uniform volume and uniform wedge models produce dispersion results almost exactly the same, consistently higher in frequency compared to the standard case. The largest discrepancy is at larger values of phase shift per turn. The on-axis interaction impedance for these models is compared in Figure 16, showing slightly higher values of impedance at low values of phase shift per turn for the approximated models compared to the standard case. The CPU for each of these models is compared in Table IV showing that there is a significant time savings with the uniform wedge and volume versus the quasi-rectangular supports.

The uniform volume and wedge models are derived from the premise that the effective permittivity of the support rods is homogeneous with the radial dimension. However, because of the radial inhomogeneous nature of the rectangular rods, this is inaccurate. To include these inhomogeneous loading characteristics, the support rods were generated as a volume and then as wedges divided into p sections with graded dielectric constants consistent with the relationship

$$\varepsilon_{rp}' = 1 + (\varepsilon_{rp} - 1)\frac{A_p}{A_p'} \tag{18}$$

where ε_{rp}' and A'_p are the effective dielectric constant and cross-sectional surface area, respectively, of the pth section of the wedges in the MAFIA model. ε_{rp} and A_p are the actual dielectric constant and cross-sectional surface area of the pth section of the actual rectangular rods. The cross-sectional views of the rod configurations for the graded volume and wedges are shown in Figure 17 and Figure 18, respectively.

Both the graded volume and wedge MAFIA models embodied p=4 sections. The dispersion and on-axis interaction impedance were calculated and are compared to measured results and those obtained with the standard model in Figure 19 and Figure 20, respectively. From these plots, it is obvious that these geometrical approximations provide results very close to the standard model. The CPU times for each of these models are compared in Table IV, showing that the graded volume and wedge cases have similar computational times compared to the uniform volume and wedge cases, but far less than the standard model.

Compared to the filament approximations, the accuracy obtained with the graded support rods is better in terms of both dispersion and on-axis interaction impedance, but the computational time is about four times as long. Thus, potential users can choose the most suitable model based on the tradeoff between accuracy and CPU time.

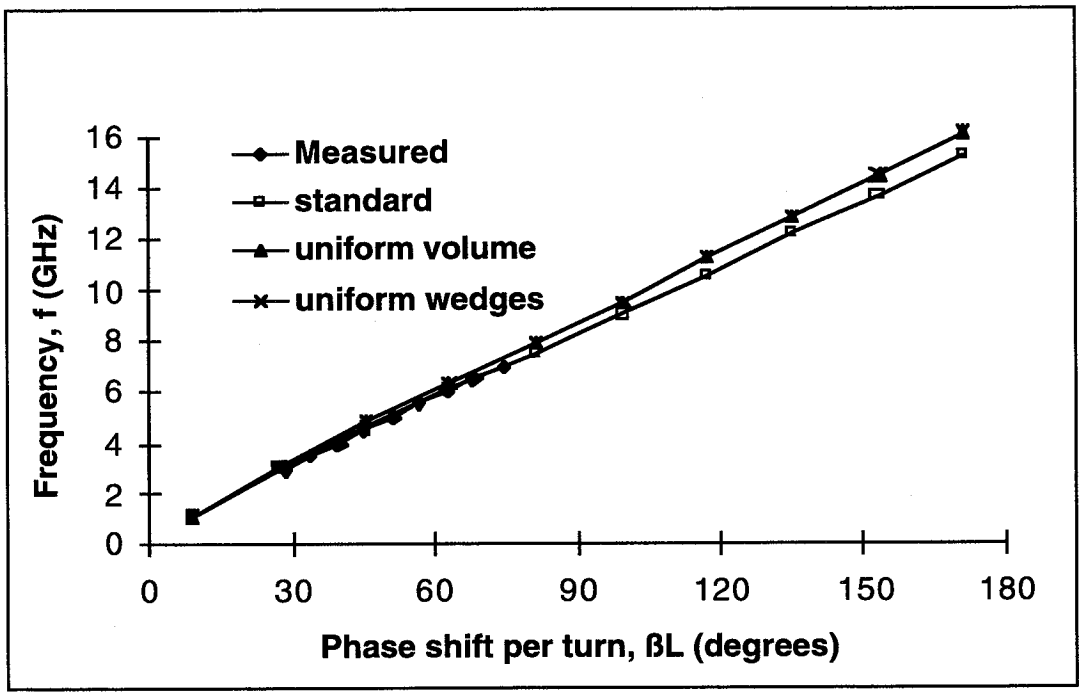

Figure 15 Measured and simulated dispersion for Northrop C-Band standard, uniform volume and uniform wedge models

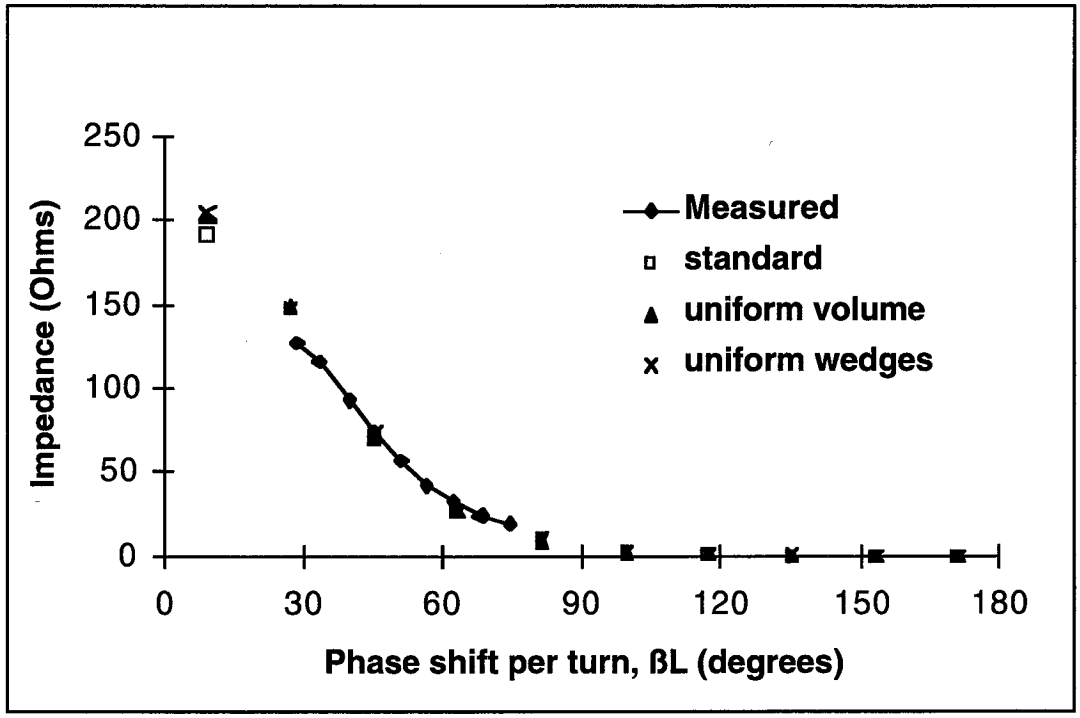

Figure 16 Measured and simulated on-axis interaction impedance for Northrop C-Band standard, uniform volume and uniform wedge models

Table IV CPU comparison for several suport rod models of ten turns of the Northrop C-Band helical circuit (RISC/6000 Model 590 Workstation)

Support Rod Configuration	CPU (hrs:mins)
Quasi-rectangular	30:05
Uniform Volume	9:04
Uniform Wedges	8:00
Graded Volume	8:36
Graded Wedges	7:56

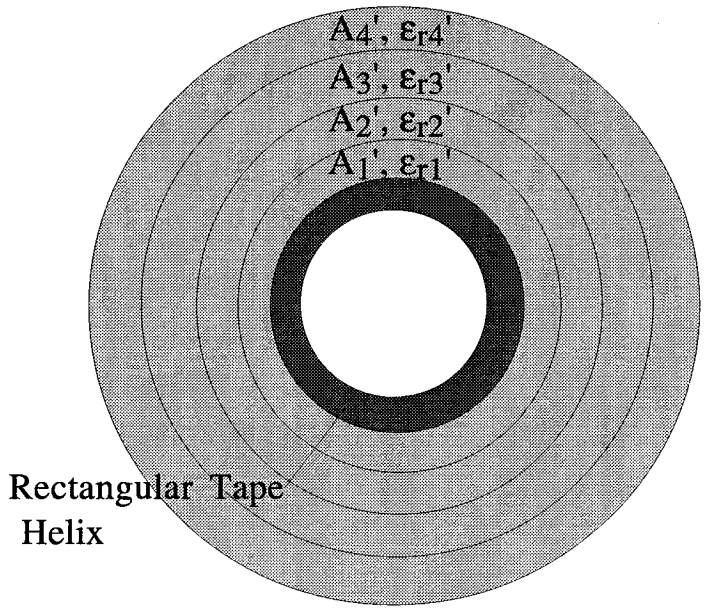

Figure 17 Northrop C-Band helical circuit graded volume support rod model

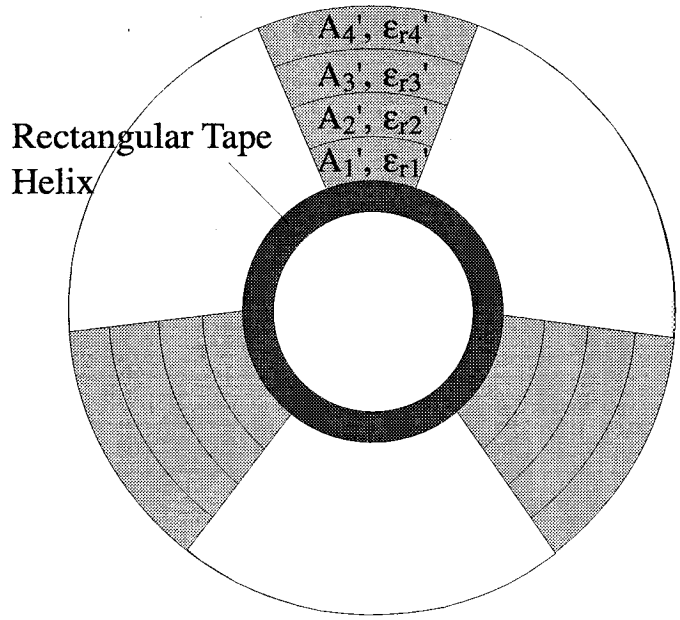

Figure 18 Northrop C-Band helical circuit graded wedge support rod model

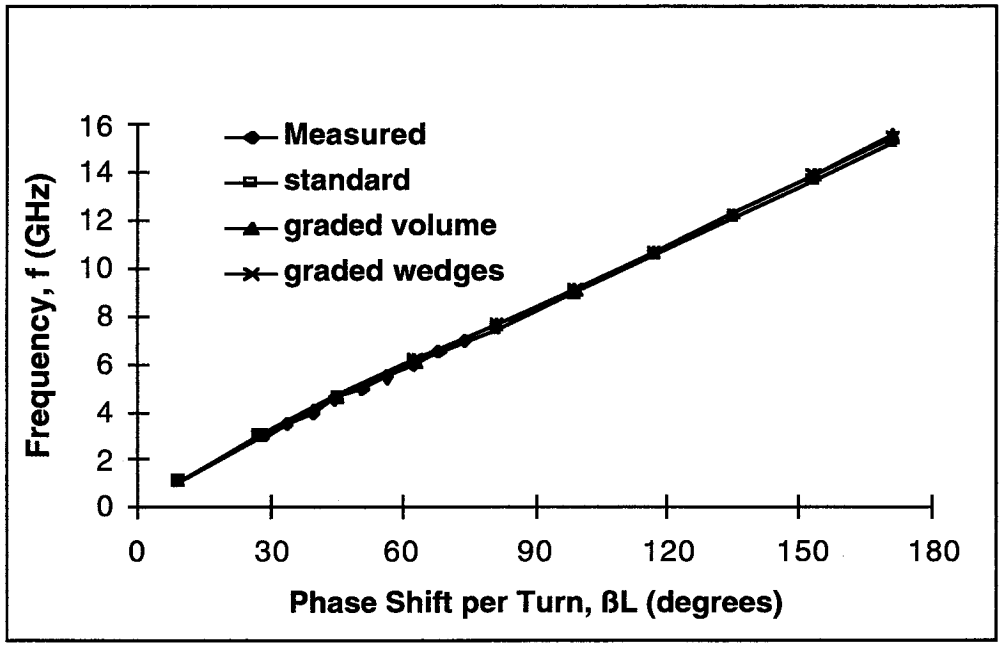

Figure 19 Measured and simulated dispersion for Northrop C-Band standard, graded volume and graded wedge models (p=4)

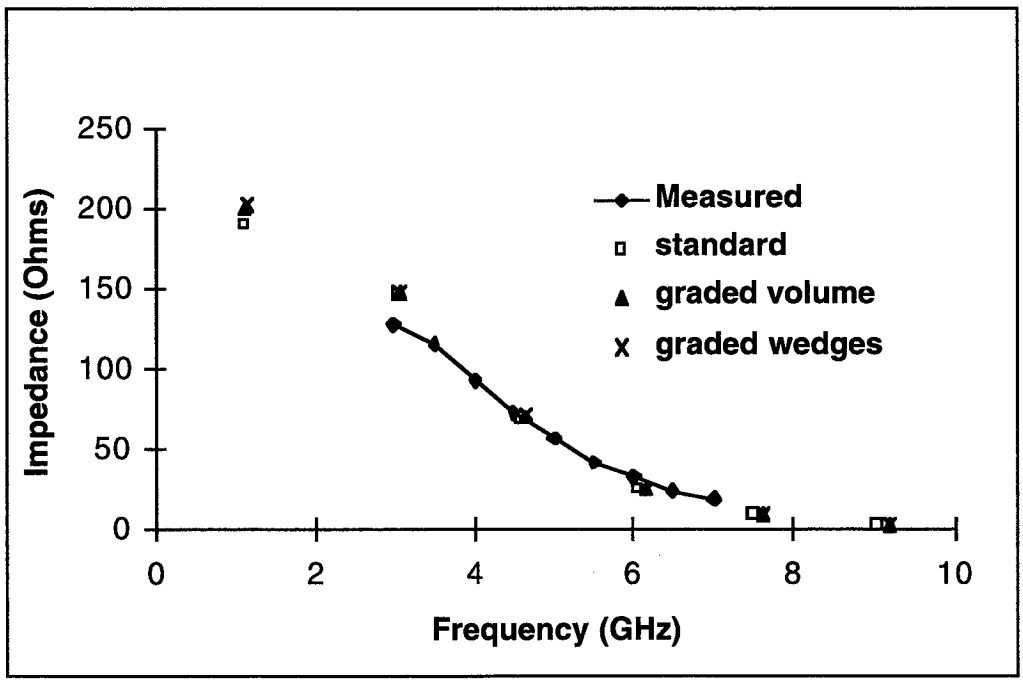

Figure 20 Measured and simulated on-axis interaction impedance for Northrop C-Band standard, graded volume and graded wedge models (p=4)

IV. BROADBAND SLOW-WAVE CIRCUIT SIMULATIONS

A Northrop Grumman broadband helical slow-wave circuit was also modeled using MAFIA and the dispersion, on-axis interaction impedance and attenuation calculated and compared with measured results [12]. The cross-sectional and longitudinal views of the circuit are shown in Figure 21. The circuit is similar to the C-Band circuit discussed in Chapter III with rectangular BeO support rods, but includes a copper film partially coating the support rods to broadband the circuit. The helical tape is made out of a tungsten/rhenium alloy. This circuit is also used as a model to investigate the sensitivity of various circuit parameters including the distance from the center of the helix to the metal film, metalr, the width of the support rods, rodw, the tape width, tapew, and the dielectric constant of the support rods, ε_r (See Figure 21).

IV.1 Cold-Test Characteristics

The broadband model includes support rods which are partially coated on each side with an infinitely conducting film. Initially the support rods were modeled using the quasi-rectangular configuration discussed in Chapter III for the C-Band circuit. With this configuration, it is necessary to use ten radial increments for the dielectric support rods to prevent the protrusion of the dielectric material through the metal coating. This increased number of radial increments, compared to six for the C-Band circuit, complicates the boundary conditions of the problem further, increasing the time for the computation to converge. Because of this added complexity and computational time, the support rods were generated in graded wedges using graded effective dielectric constants consistent with Equation 18 as discussed in Chapter III, where it was shown that there was a significant savings in computational time with negligible change in dispersion and on-axis interaction impedance. Figure 22 shows the cross-sectional view of the Northrop broadband circuit graded wedge model. The number of sections p was again chosen to be four. Figure 23 shows a MAFIA electric field plot of the cross-sectional view of the broadband circuit, the size of the arrows proportional to the magnitude of the field. It is apparent that the electric fields are concentrated more between the helix and the beginning of the metal film than in the region extending from the film to the barrel. Thus, the section of the support rods extending radially from the helix to the metal radius was divided into three regions, and the section from the metal radius to the barrel was treated as one region. A three-dimensional MAFIA plot of several turns of the Northrop broadband helical slow-wave structure is shown in Figure 24. An azimuthal increment of 20 degrees was used to model the helical tape.

IV.1.1 Dispersion

A comparison of the measured and simulated dispersion is shown in Figure 25. Very good agreement was obtained across the bandwidth, the average absolute difference between measured and simulated results being about 1.5%.

IV.1.2 On-Axis Interaction Impedance

The on-axis interaction impedance was calculated according to Equation 11 and compared to measured results in Figure 26. The impedance calculated using MAFIA is consistently lower by an average difference of about ten Ohms.

IV.1.3 Attenuation

The attenuation values calculated using MAFIA are compared with measured values in Figure 27. The loss tangent for BeO was taken to be .0001 and the conductivity of the tape was initially approximated to be consistent with twice the resistivity of the theoretical value for tungsten, in line with [18] as described previously. The conductivity of the copper loading film was also kept consistent with twice the resistivity of the theoretical value for copper. When these values were used, the attenuation obtained using MAFIA was lower than experimental data. It was found that using a value 2.46 times the theoretical resistivity value of tungsten

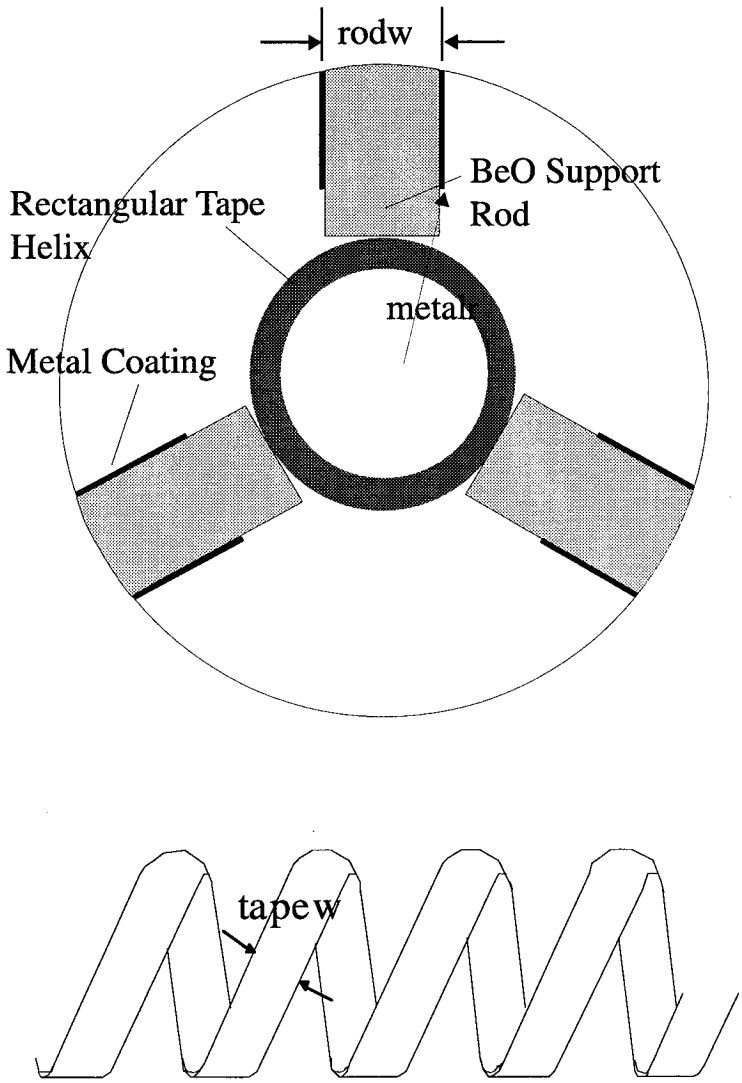

Figure 21 Northrop Grumman broadband helical TWT slow-wave circuit

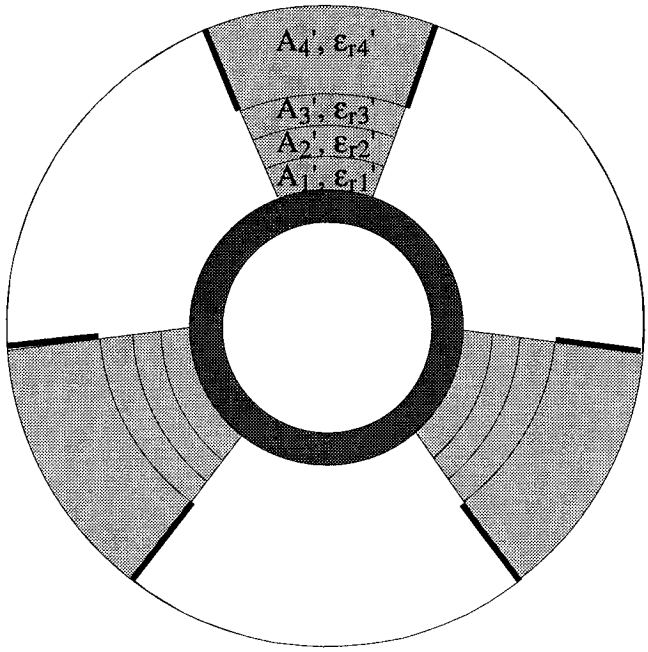

Figure 22 Northrop broadband helical slow-wave circuit model with graded wedge support rods

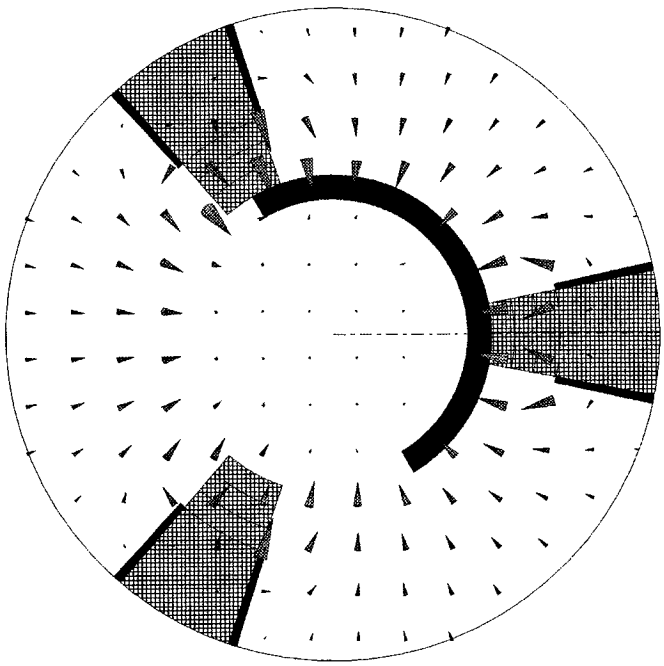

Figure 23 MAFIA electric field plot of cross-section of Northrop broadband helical circuit (βL = 9 degrees)

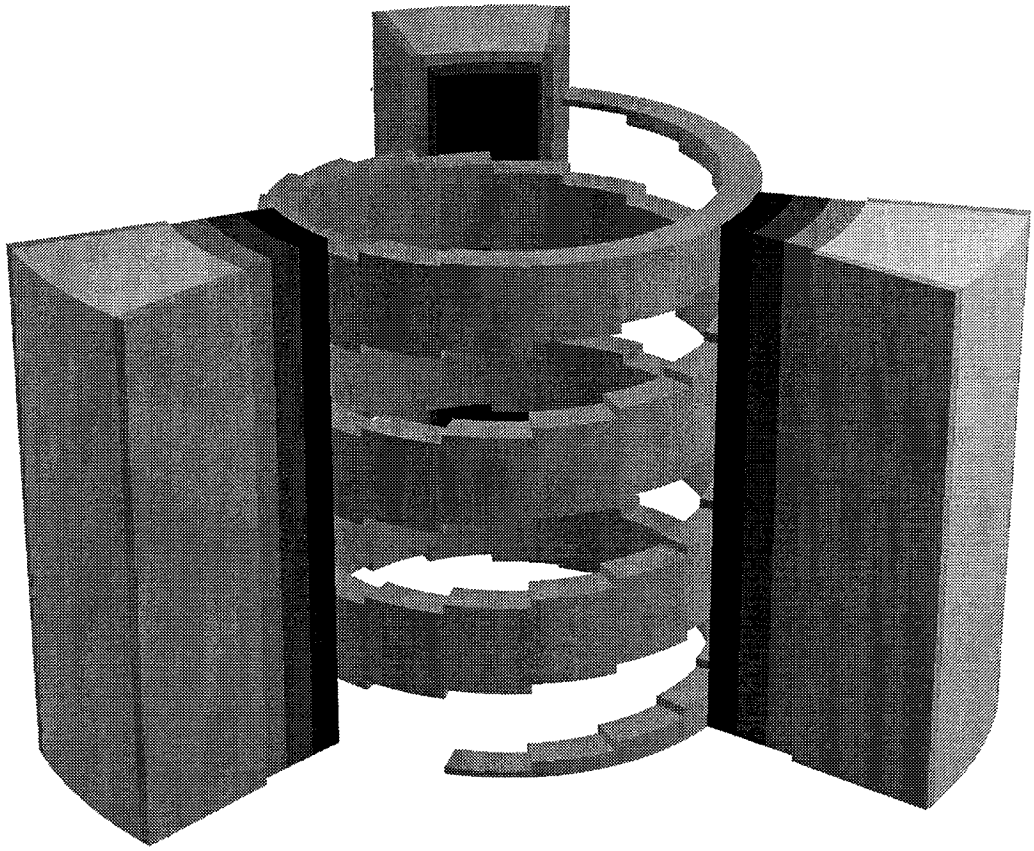

Figure 24 MAFIA three-dimensional plot of several turns of the Northrop broadband helical circuit

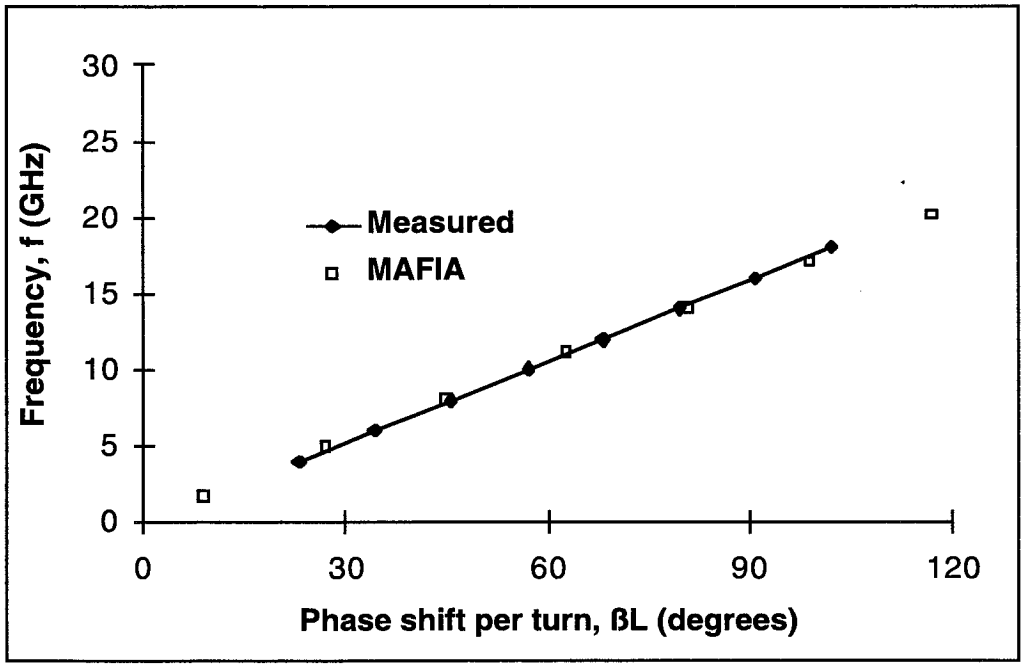

Figure 25 Measured and simulated dispersion for Northrop broadband helical circuit

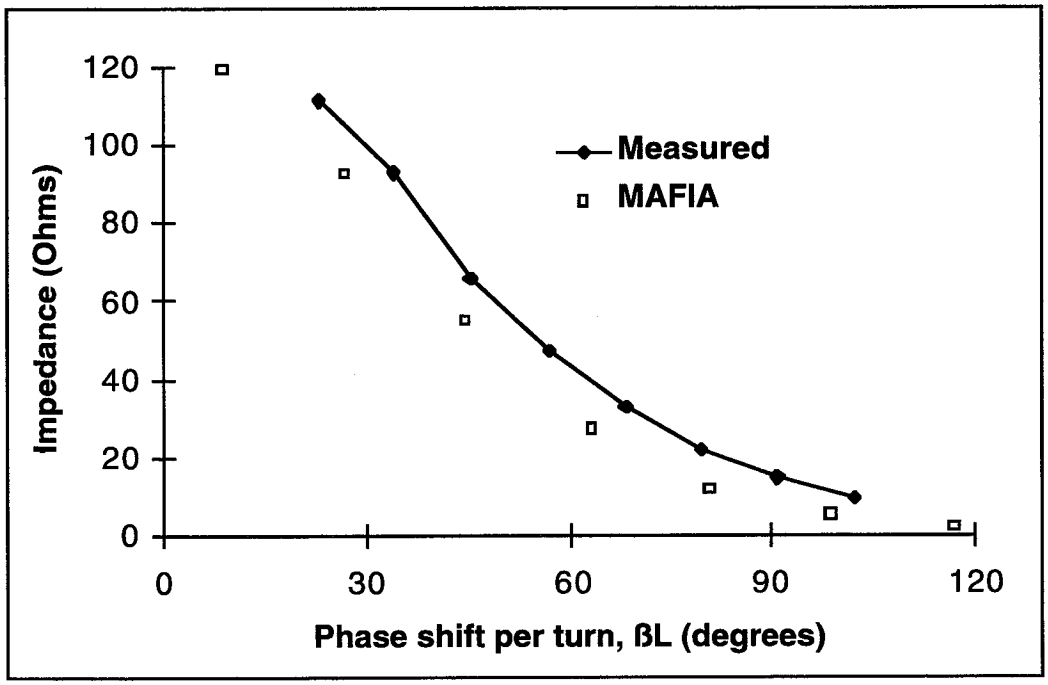

Figure 26 Measured and simulated on-axis interaction impedance for Northrop broadband helical circuit

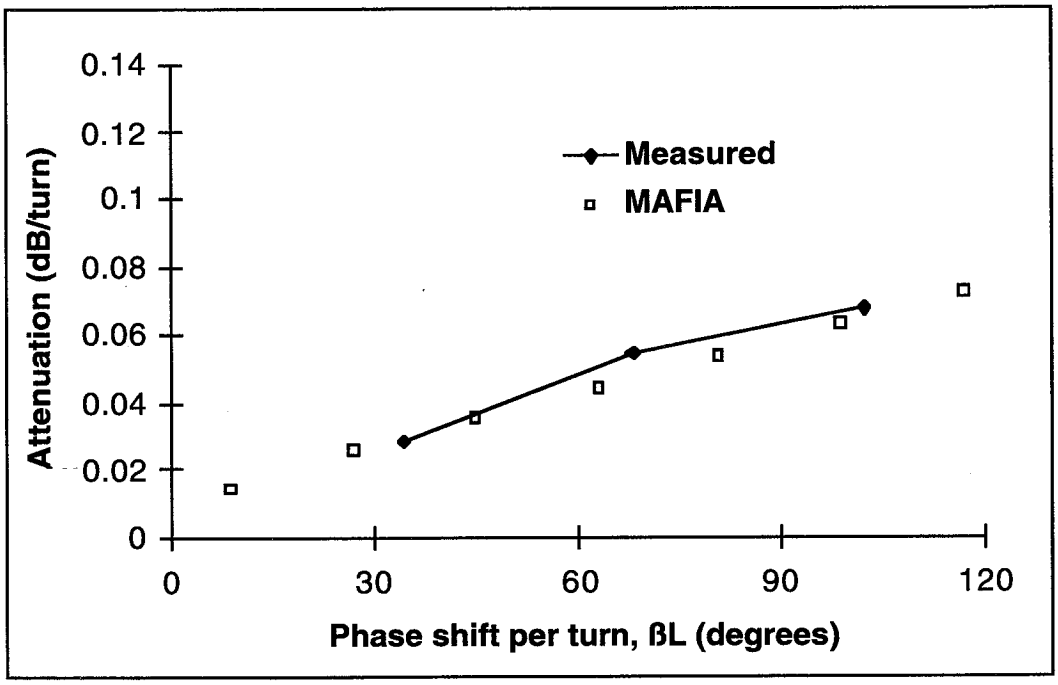

Figure 27 Measured and simulated attenuation for Northrop broadband helical circuit

for the helical tape gave the best agreement with measured attenuation as is shown in Figure 27 with an absolute average difference in attenuation of .003 dB/turn. This lower conductivity value for the tape might be expected as the helix was actually fabricated from a tungsten/rhenium alloy containing about 3% rhenium. Relevant experimental data for the conductivity was not available, but conductivity for the alloy would be less than the value for pure tungsten, so this factor of 2.46 is not unreasonable.

IV.2 Circuit Parameter Sensitivity

Unfortunately, it is not an uncommon experience that TWT's of the same model, presumably fabricated within manufacturing tolerances, exhibit significant variations in performance. These variations represent a considerable cost to the industry, particularly when they are large enough that completed TWT's do not meet specifications. It would seem likely that these variations are the result of inadequately controlled manufacturing processes, but an accurate investigation of this hypothesis has been impossible until recently. This section demonstrates the variations that can occur in TWT performance when the permittivity of the support rods and key dimensions of the slow-wave structure vary within and beyond the tolerances typically employed within the industry.

The Northrop MPM broadband circuit was chosen for this analysis because it represents most of the elements of a modern slow-wave structure design, including a tape helix supported by metallized rectangular support rods, and because a complete set of dimensions and experimental data were available from the manufacturer. The dimensions analyzed were the width and relative dielectric constant of the support rods, rodw and ε_r, respectively, the distance from the helical axis to the beginning of the metal film deposited on the dielectric rods, metalr, and the width of the helical tape, tapew (see Figure 21). The sensitivity of these parameters are compared in terms of the normalized phase velocity and on-axis interaction impedance. The dispersion is compared in the form of normalized phase velocity so the effect on bandwidth is apparent in the results.

The specific results presented here apply only to the mentioned circuit; however, these results can serve as a general guide for similar devices, and the computational techniques described here are readily applicable to other TWT's. Based on this kind of information, manufacturers can conduct cost-benefit analyses of their manufacturing tolerances.

IV.2.1 Metal Film Radius

First the dispersion and on-axis interaction impedance were calculated for several variations on the metal film radius, metalr of Figure 21. The dimension was varied within and beyond its manufacturing tolerance of 0.0005 inches. The results are plotted for the dispersion in Figure 28. From this plot we see that as the film approaches the helix, or the loading is increased, the bandwidth is increased. Figure 29 which plots the on-axis interaction impedance for the same variations, shows that this increase in bandwidth is achieved at the expense of a decreased impedance.

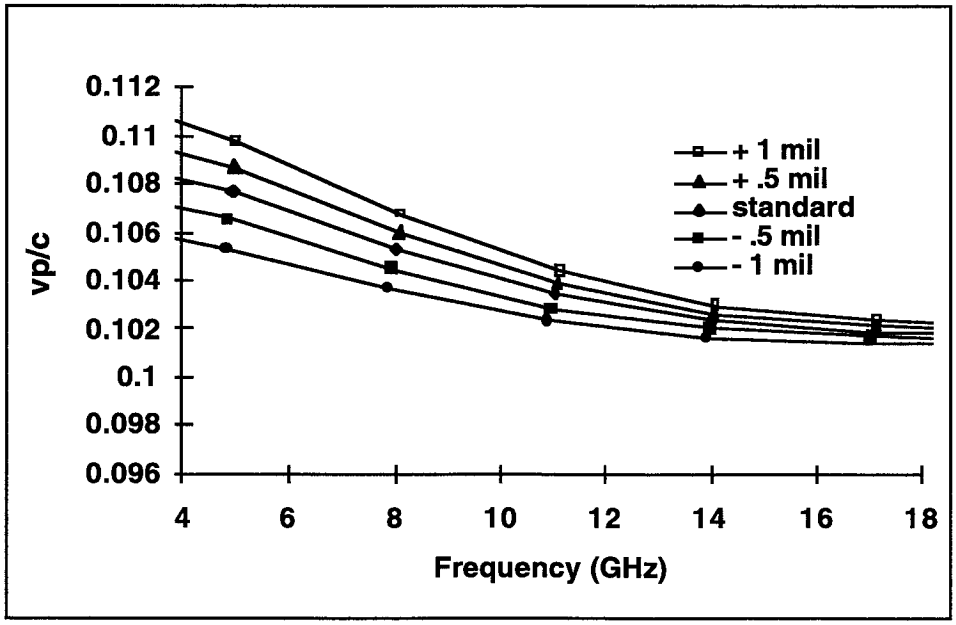

Figure 28 Simulated dispersion for variations on metal film radius, metalr, for Northrop broadband helical circuit

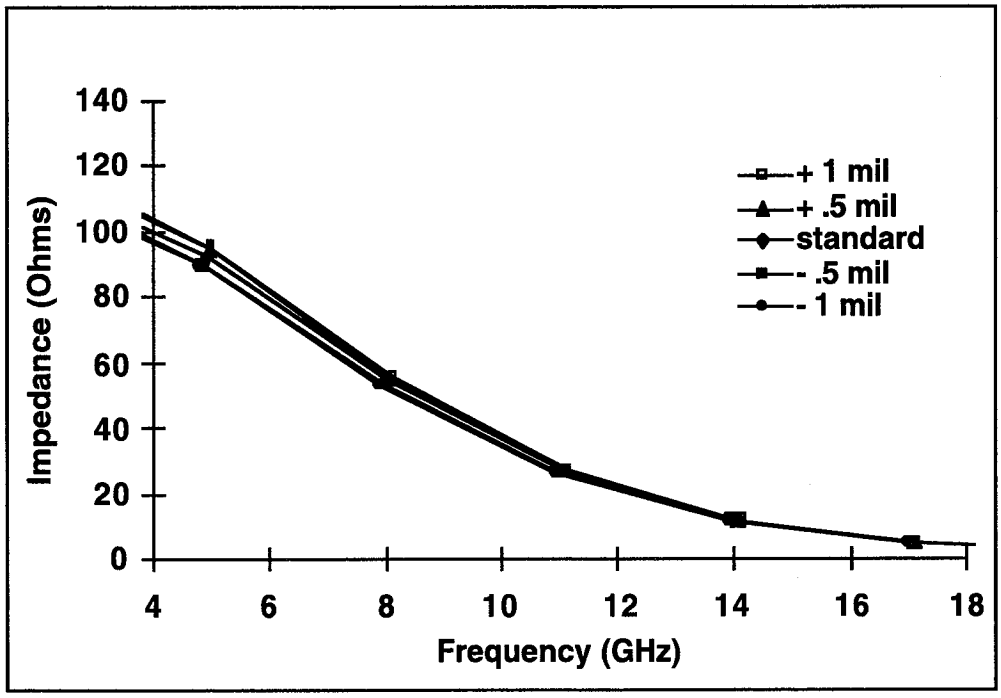

Figure 29 Simulated on-axis interaction impedance for variations on metal film radius, metalr, for Northrop broadband helical circuit

IV.2.2 Support Rod Width

Next, the dispersion and on-axis interaction impedance were calculated for several variations on the support rod width (rodw of Figure 21). Figure 30 and Figure 31 show the dispersion and on-axis interaction impedance, respectively, for variations within and beyond its manufacturing tolerance of 0.0005 inches. From these plots we see that these variations will not affect bandwidth, but will increase or decrease the phase velocity, and thus the operating voltage, uniformly across the bandwidth. The impedance is also uniformly increased or decreased across the bandwidth, increasing slightly when the rod is made thinner.

IV.2.3 Helical Tape Width

The axial width of the helical tape, tapew, was varied within and beyond its dimensional tolerance of .0005 inches. Figure 32 and Figure 33 show the dispersion and on-axis interaction impedance, respectively. With increased tape width, only a slight decrease in both phase velocity and impedance occurs uniformly across the bandwidth except for the + 1 mil variation which decreases the phase velocity more significantly.

IV.2.4 Support Rod Permittivity

Lastly, the relative dielectric constant of the support rods was varied. The motivation for this last set of variations was based on citations from various sources that reported the dielectric constant for BeO to be anywhere from 6 to 7.5. As part of another investigation, we have already done some in-house dielectric measurements on APBN where we found variations in the permittivity as high as +/- 10% within the same sample [20]. We intend to also conduct an experimental study of the permittivity of BeO.

Figure 34 and Figure 35 show the dispersion and on-axis interaction impedance, respectively, for variations on the dielectric constant from 6 to 7.5, the nominal value for BeO being 6.5. The difference in the dispersion and impedance is greater than any of the dimensional variations made, even those beyond the dimensional tolerances. This could be a large contributing factor to why TWT's of the same model, presumably fabricated within manufacturing tolerances, exhibit significant variations in performance. From these results it appears the phase velocity and impedance are uniformly shifted up or down across the bandwidth. With increasing permittivity, phase velocity and impedance decrease.

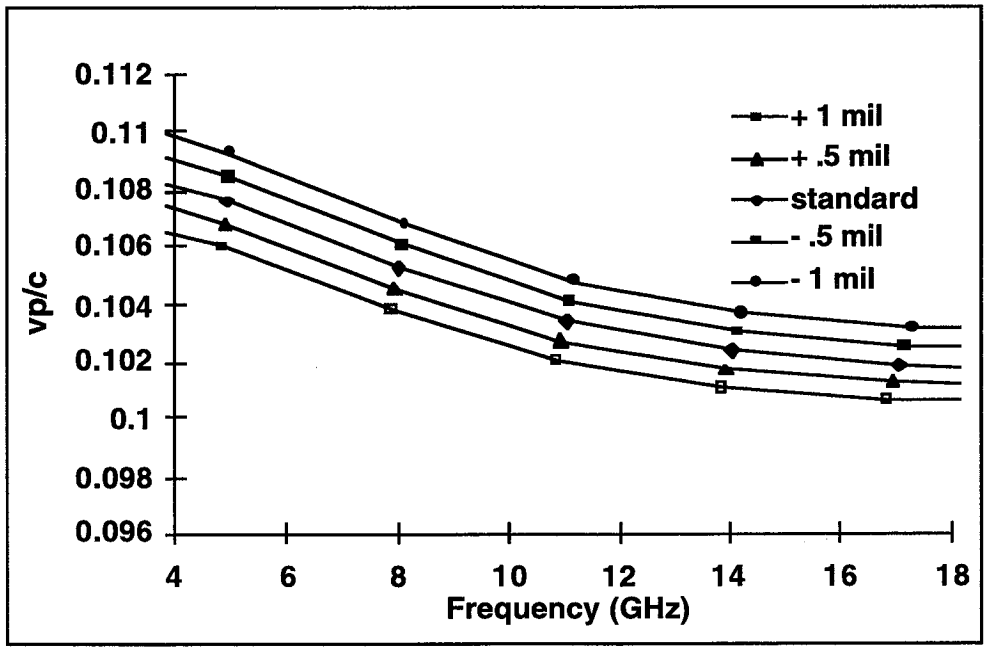

Figure 30 Simulated dispersion for variations on support rod width, rodw, for broadband helical circuit

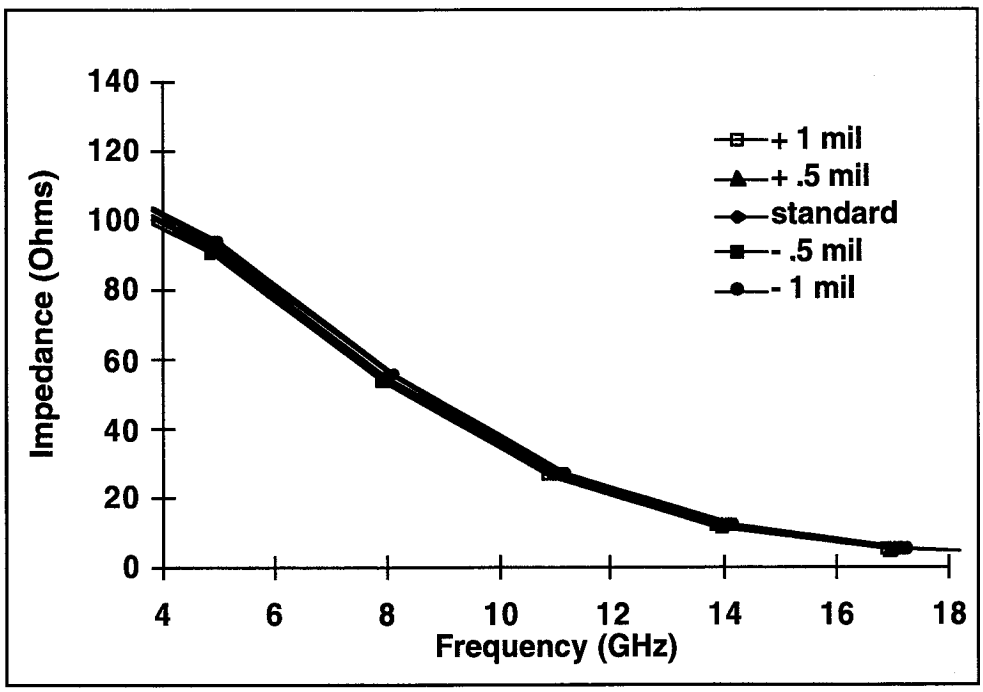

Figure 31 Simulated on-axis interaction impedance for variations on support rod width, rodw, for broadband helical circuit

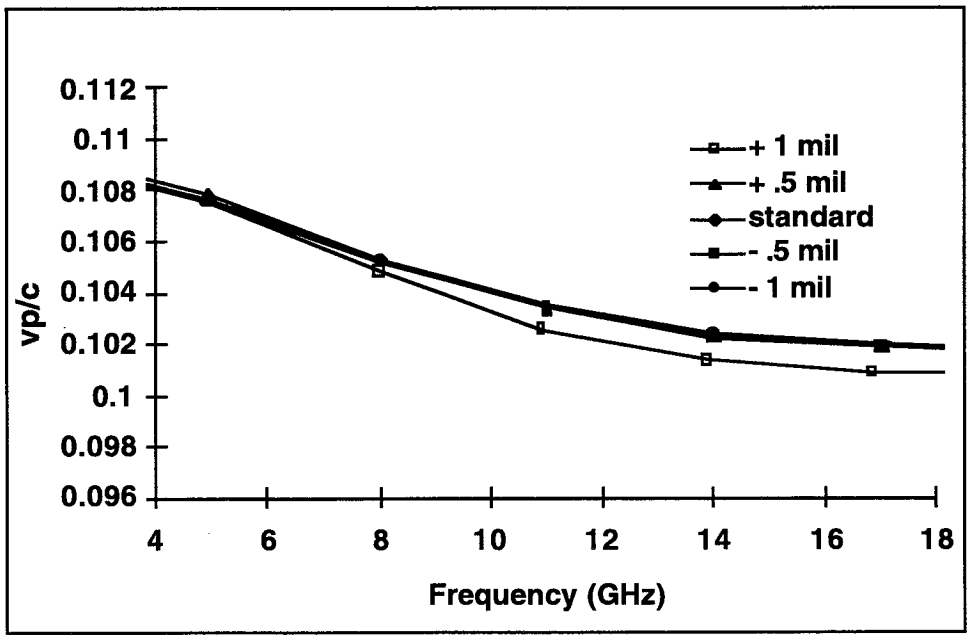

Figure 32 Simulated dispersion for variations on helical tape width, tapew, for broadband helical circuit

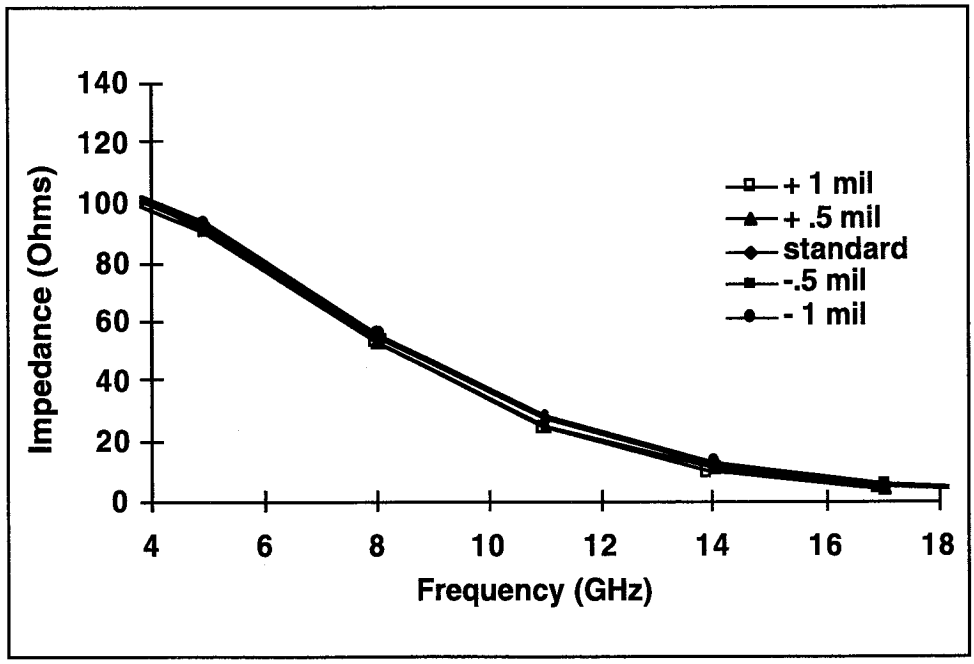

Figure 33 Simulated on-axis interaction impedance for variations on helical tape width, tapew, for Northrop broadband helical circuit

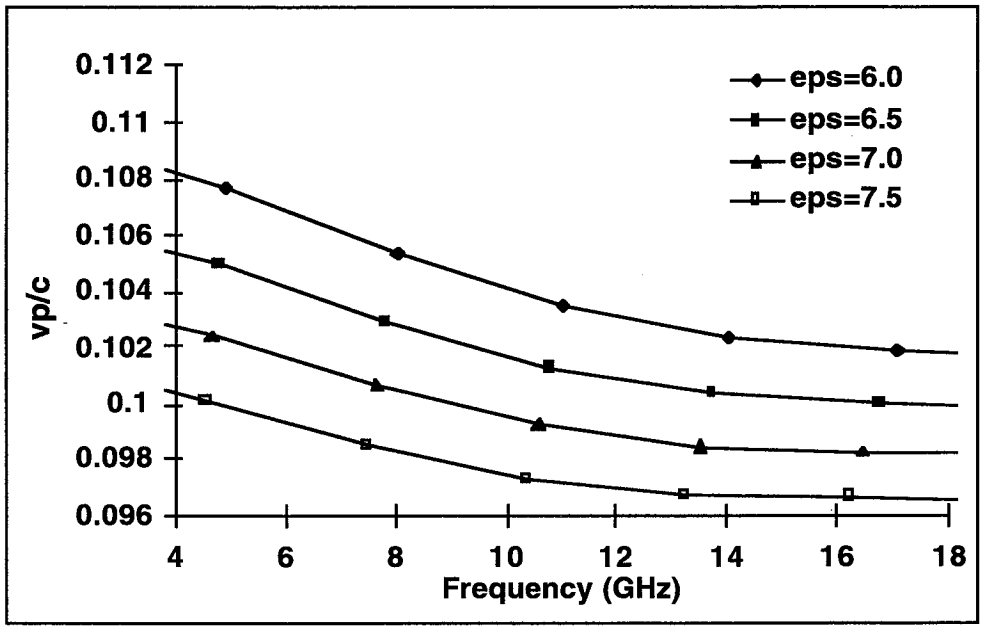

Figure 34 Simulated dispersion for variations on support rod permittivity, ε_r, for Northrop broadband helical circuit

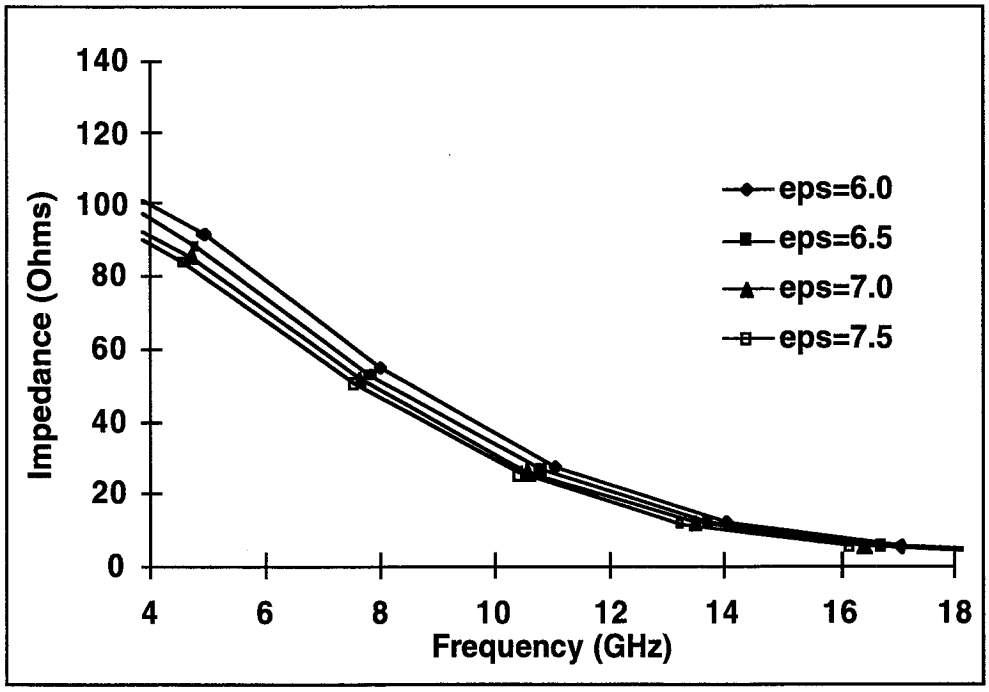

Figure 35 Simulated on-axis interaction impedance for variations on support rod permittivity, ε_r, for Northrop broadband helical circuit

V. ADDITIONAL SIMULATIONS

Two additional TWT slow-wave circuits were modeled to demonstrate how MAFIA can be used to study circuits having more complex geometries and material characteristics. Included in the study is a circuit with APBN support rods to demonstrate the capability of modeling anisotropic materials, and a circuit with T-shaped dielectric support rods.

V.1 Anisotropic Dielectric Support Rods

The circuit discussed here is the helical slow-wave circuit from a 10 Watt, 32 GHz traveling-wave tube amplifier (TWTA) for incorporation into the Ka-Band Transmitter package for the Cassini mission [13]. It embodies a rectangular, copper plated tungsten/rhenium, helical tape supported by rectangular anisotropic pyrolytic boron nitride (APBN) rods oriented for low RF losses rather than thermal conductivity. The circuit resembles the Northrop Grumman C-Band circuit of Figure 2. Similarly, the support rods were generated in the cylindrical coordinate system by using six radial increments by reducing the rod angle with increasing radius, or the quasi-rectangular configuration. The helix itself was generated with an azimuthal increment of 20 degrees. Only the measured dispersion and attenuation were available from the manufacturer for comparison.

V.1.1 Dispersion

For this circuit with the APBN support rods, the nominal dielectric constant is 5.1 parallel to the layers and 3.4 perpendicular. Since the rods are oriented for low RF losses rather than thermal conductivity, this implies an effective dielectric constant of 5.1 in the azimuthal and axial directions, and 3.4 in the radial direction. Using these nominal values, the dispersion

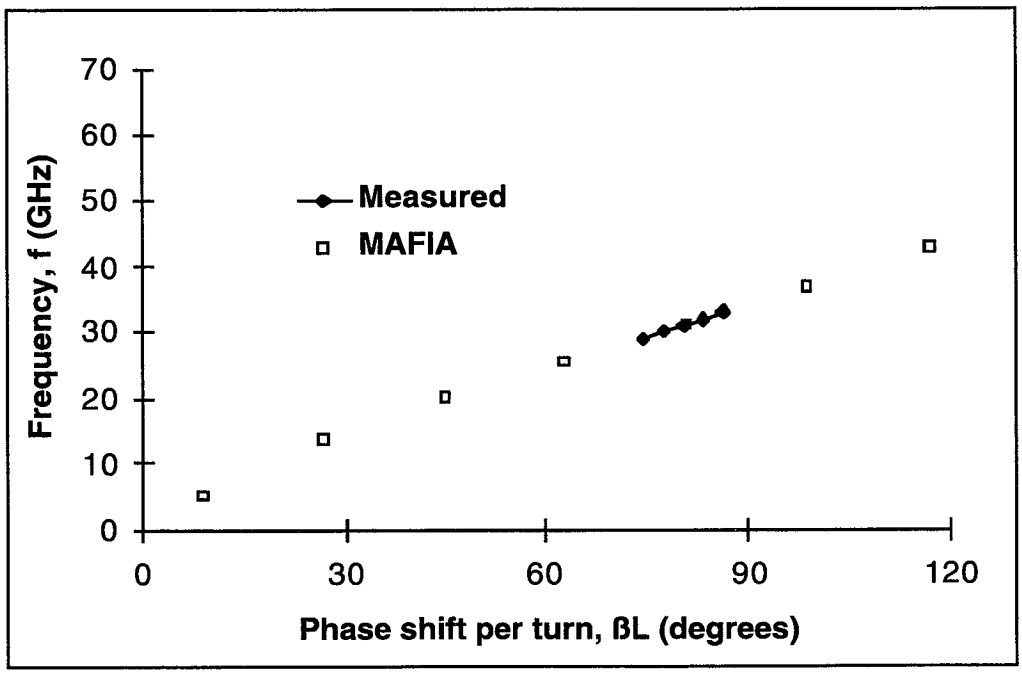

Figure 36 Measured and simulated dispersion for Cassini helical circuit

obtained using MAFIA was consistently lower than measured values by about one GHz, or an absolute frequency difference of about 3%. By varying the relative dielectric constant of the rods to 4.6 in the azimuthal and axial directions, and 2.3 in the radial direction, the results shown in Figure 36 were obtained. The average absolute difference across the bandwidth between measured dispersion and that obtained using MAFIA is only 0.6%.

As mentioned, some in-house measurements of APBN showed that the permittivity can vary within the same plate of material from the same manufacturer by as much as +/- 10% [20]. With this information, the variations made from the nominal permittivity values for the Cassini support rods are approximately justified. Unfortunately, it is impossible to establish the exact anisotropic permittivity of the dielectric rods used in these already assembled tubes.

V.1.2 Attenuation

The attenuation was also calculated for the Cassini circuit using a conductivity value of 2.25×10^7 S/m for the helical tape, nearly the theoretical value of pure copper, and compared with measured values in Figure 37. Much attention was given to polishing the helical tape to a bright, shining finish; therefore, this large conductivity value is explained.

V.2 T-Shaped Dielectric Support Rods

The last circuit modeled was the helix slow-wave circuit from a Hughes TWT for the MPM [14]. The experimental circuit includes a rectangular, copper plated helical tape supported by T-shaped BeO rods inside a conducting barrel as shown for the end view in Figure 38. A MAFIA three-dimensional plot of several turns of the helical circuit is shown in Figure 39. The azimuthal increment used to generate the helical tape is 20 degrees. Only the measured dispersion was available from the manufacturer for comparison.

V.2.1 Dispersion

The dispersion was calculated for the Hughes helical circuit and shown in Figure 40. The results using MAFIA agree very well with measured data with an absolute average difference across the bandwidth of 1.8%

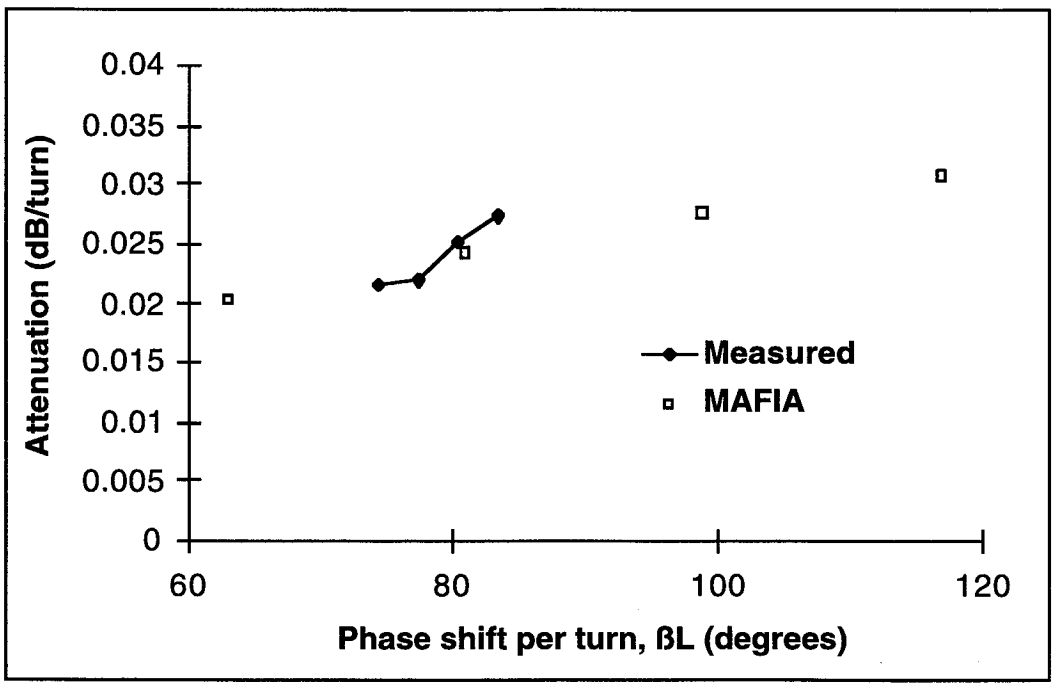

Figure 37 Measured and simulated attenuation for Cassini helical circuit

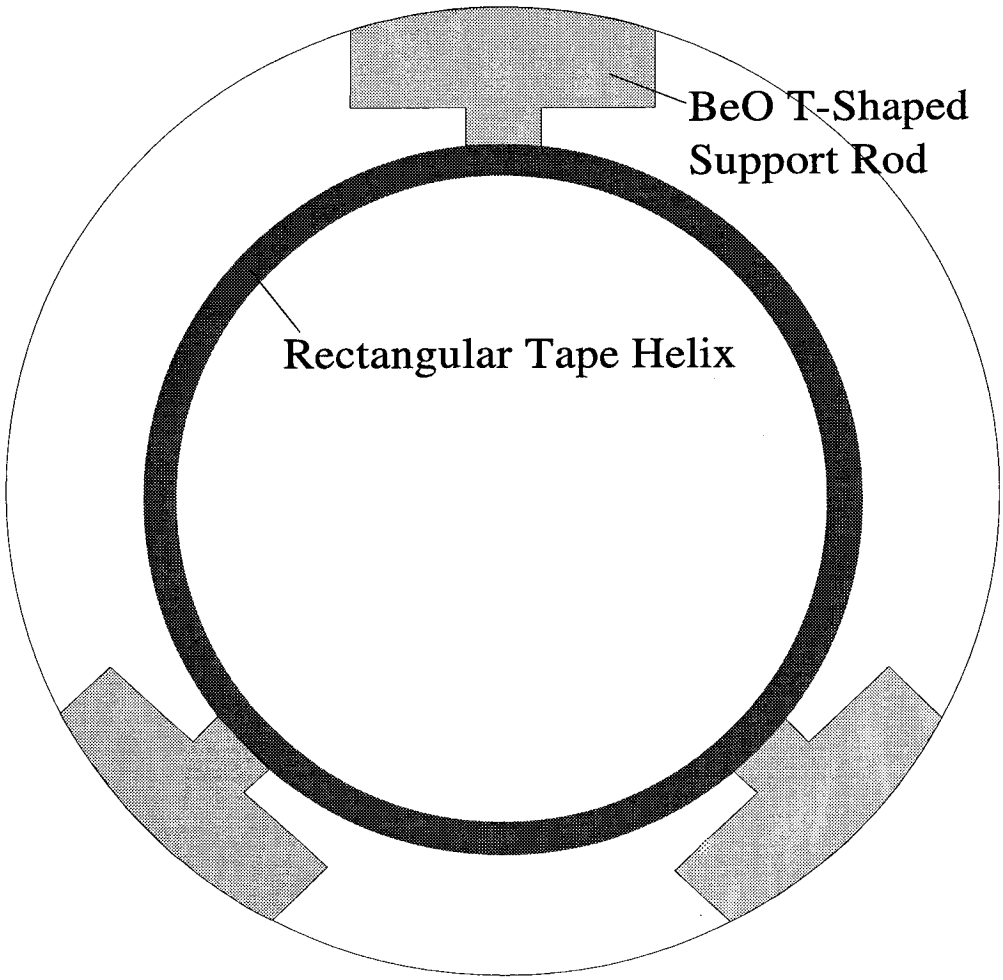

Figure 38 Hughes MPM helical slow-wave circuit

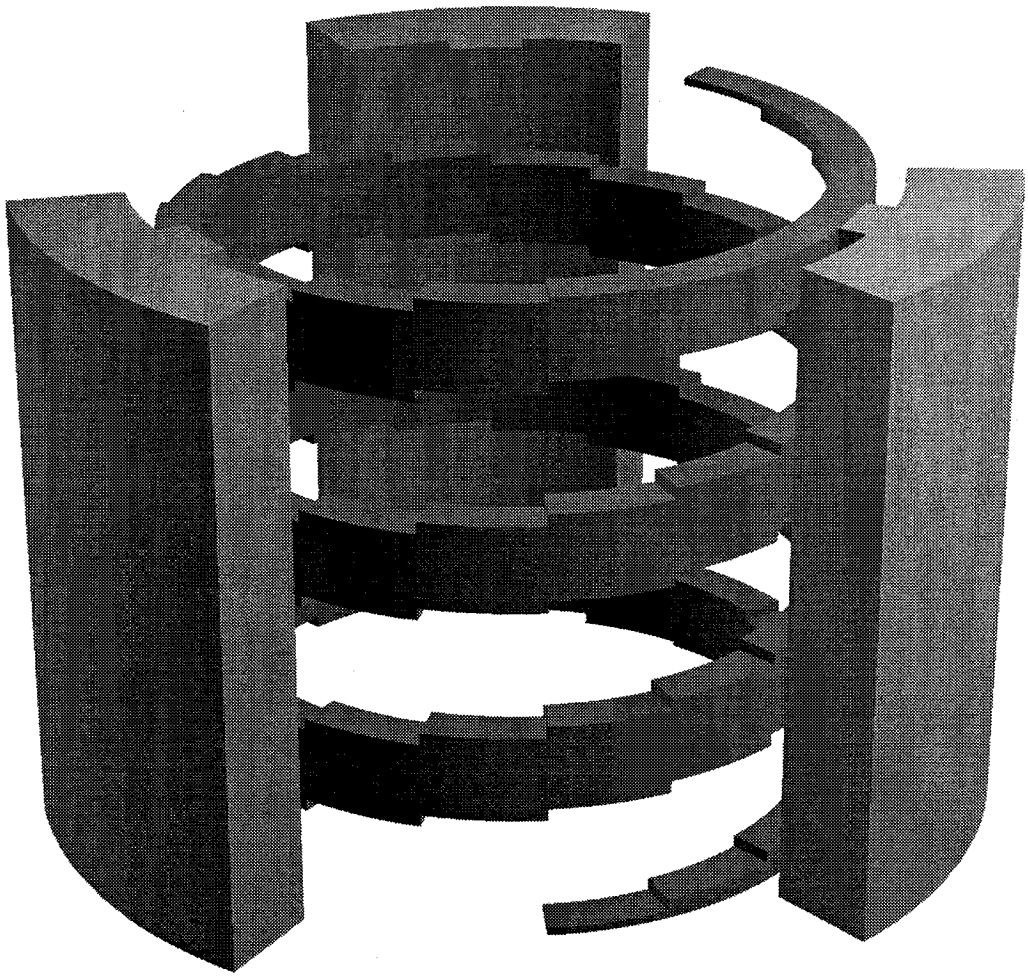

Figure 39 MAFIA three-dimensional plot of several turns of the Hughes MPM helical circuit

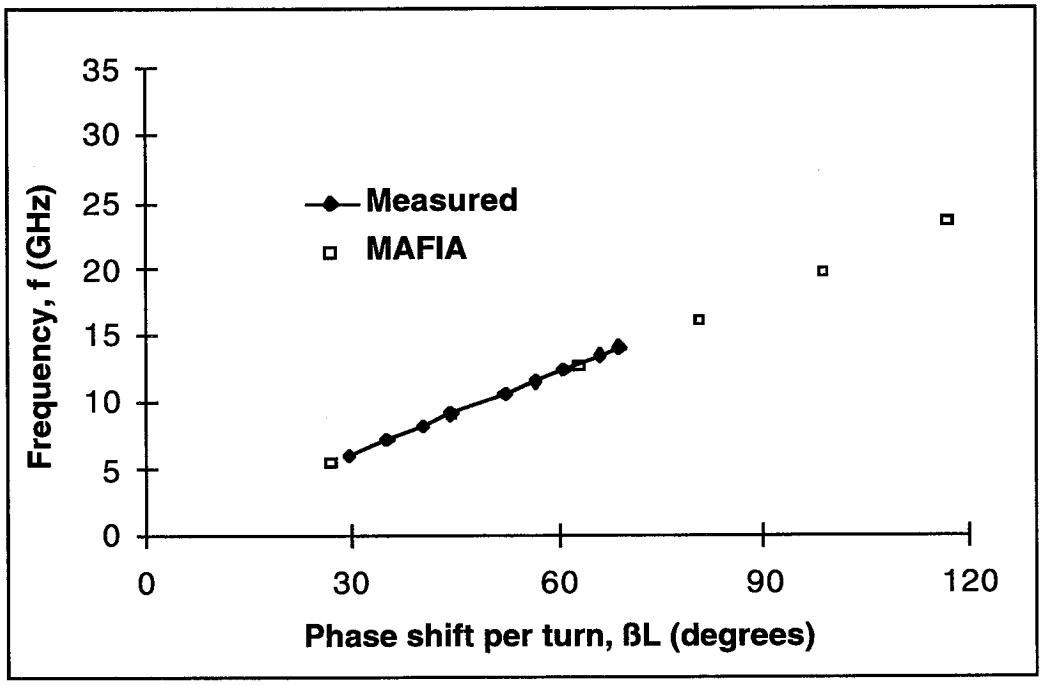

Figure 40 Measured and simulated dispersion for Hughes MPM helical circuit

VI. CONCLUSIONS

An accurate three-dimensional TWT helical slow-wave circuit model has been introduced and the accuracy validated by comparing measured cold-test results with those obtained using MAFIA with excellent agreement. First an in depth analysis was given describing how MAFIA can be used to obtain the cold-test characteristics including dispersion, on-axis interaction impedance and attenuation. Then, the simulated results for several TWT helical slow-wave structures were presented.

The Northrop Grumman C-Band helical circuit, representing one of the most basic helical slow-wave structure designs, was modeled first. The cold-test results using MAFIA show excellent agreement when compared to measured values with absolute average differences across the bandwidth of 0.7%, six Ohms and .0005 dB/turn, for the dispersion, impedance and attenuation, respectively. The CPU time to simulate ten turns of this standard MAFIA C-band model is about 30 hours.

In an attempt to obtain the most computationally efficient model, several geometric approximations were made to the standard C-band helical circuit model. It was found that replacing the helical tape with a series of infinitesimally thin, perfectly conducting filaments placed uniformly in the radial and axial direction to "cage in" the helix significantly reduces the CPU time to about two hours. Unfortunately, the dispersion is significantly lower, especially at higher frequencies, and the impedance is consistently higher, notably at lower frequencies. Although this model provides approximate results, the large savings in CPU time make it a candidate to be used to simulate an entire tube, or section of a tube. With the standard model, this would be impossible because of the computational intensity.

It was found that replacing the quasi-rectangular support rods of the standard model with graded volume or graded wedges reduces the CPU time to about eight hours, with only a slight change in both the dispersion and impedance.

Next the cold-test characteristics for the Northrop Grumman broadband helical circuit were presented and compared to measured data with absolute average differences across the bandwidth of 1.5%, ten Ohms and .003 dB/turn, for the dispersion, impedance and attenuation, respectively. To demonstrate how MAFIA can be used to investigate the sensitivity of various circuit parameters, the dispersion and on-axis interaction impedance were compared for variations on the helical tape width, metal film radius and the width and permittivity of the support rods. It was found that as the distance from the helix axis to the metal film is decreased the bandwidth increases, but the impedance consequently decreases. Making the support rods thinner uniformly increases the phase velocity and impedance across the bandwidth. Varying the tape width has a small effect on both dispersion and impedance. Because a helix fabricated with wider tape width would have improved thermal properties, this result may have valuable engineering significance. Variations on the support rod permittivity has a larger effect on both the dispersion and impedance than any of the other variations made, even those beyond the dimensional tolerances. These results could be a large contributing factor to why TWT's of the same model, presumably fabricated within manufacturing tolerances, exhibit significant variations in performance.

Two additional helical slow-wave circuits were modeled using MAFIA, the Ka-Band circuit from the TWTA for the Cassini mission and the Hughes MPM circuit embodying T-shaped support rods. The results for the Cassini circuit using MAFIA, compared to measured data, show an absolute average difference across the operating range of 0.6% for the dispersion. The conductivity value used in the MAFIA simulation for the helical tape was obtained by matching the measured attenuation with experimental data. The conductivity for the helical tape was found to be 2.25x107 S/m, very close to the theoretical value of copper, indicating a very smooth helical surface. An absolute average difference of 1.8% across the operating range was obtained for the dispersion for the Hughes MPM helical circuit.

A discrepancy in the agreement between the on-axis interaction impedance supplied from industry and that calculated using MAFIA is expected since the methods used to calculate this cold-test parameter differ. To experimentally obtain on-axis interaction impedance, the circuit is perturbed with a small dielectric rod at the center of the helical axis, and the change in phase shift between the perturbed and unperturbed circuit at a constant driving frequency is measured. From Slater's perturbation theory, the formula for on-axis interaction impedance is derived [21]. Several approximations go into this derivation, the accuracy of which will be investigated using MAFIA. Also the effect of the misalignment of the perturbing rod and variation in rod permittivity and size on impedance will be investigated.

A more in depth study of the effects of support rod permittivity on TWT performance will be completed by simulating several variations to the dielectric constant of the rods, including axially and azimuthally asymmetric configurations, consistent with likely variations occurring in actual manufactured TWT's.

Lastly the effect that altering the diameter or pitch of the helical tape on TWT performance, especially impedance, will be examined. Typically, when slow-wave circuit velocity tapers are designed, it is assumed that the impedance stays constant with the altered helical pitch or diameter. Using MAFIA, the accuracy of this assumption can be determined.

ACKNOWLEDGMENT

The author would like to express her appreciation to Dr. Jeffrey D. Wilson who introduced her to this field of study and acted as her mentor, to Dr. James A. Dayton, Jr. who gave valuable guidance throughout the work and to her advisor, Dr. A. Haq Qureshi.

BIBLIOGRAPHY

1. TWT/TWTA Handbook, Hughes Aircraft Company, Electron Dynamics Division, Torrance, CA.
2. C. L. Kory and J. D. Wilson: Three-Dimensional Simulation of Traveling-Wave Tube Cold-Test Characteristics Using MAFIA, NASA TP–3513, May 1995.
3. C. L. Kory and J. D. Wilson: Novel High-Gain, Improved Bandwidth, Finned-Ladder V-Band Traveling-Wave Tube Slow-Wave Circuit Design, *IEEE Trans. on Electron Devices,* vol. 42, no. 9, pp. 1686–1692, September 1995.
4. J. R. Pierce: Traveling-Wave Tubes. Van Nostrand, New York, 1950.
5. S. Sensiper: Electromagnetic Wave Propagation on Helical Conductors, *Proc. IRE*, vol. 43, pp. 149–161, 1955.
6. P. K. Tien: Traveling-Wave Tube Helix Impedance, *Proc. IRE*, vol. 41, pp. 1617–1623, November 1953.
7. J. B. McMurtry: Fundamental Interaction Impedance of a Helix Surrounded by a Dielectric and a Metal Shield, *IRE Trans. on Electron Devices*, vol. ED-9, pp. 210–216, 1962.
8. P. K. Jain and B. N. Basu: The Inhomogeneously Loaded Effects of Practical Dielectric Supports for the Helical Slow-Wave Structure of a TWT, *IEEE Trans. on Electron Devices,* vol. ED-34, no. 12, pp. 2643–2648, December 1987.
9. A. K. Sinha et al.: Simplified Tape Model of Arbitrarily-Loaded Helical Slow-Wave Structures of a Traveling-Wave Tube, *Proc. IEE*, pt-H, vol. 139, pp. 347–350, 1992.
10. T. Weiland: On the Numerical Solution of Maxwell's Equations and Applications in the Field of Accelerator Physics, Part. Accel., vol 15, pp. 245–292, 1984.
11. T. Weiland: On the Unique Numerical Solution of Maxwellian Eigenvalue Problems in Three Dimensions, Part. Accel., vol. 17, pp. 227–242, 1985.
12. Personal communication with Gary Groshart of Northrop Grumman Corp., Electronics Systems Division.
13. A. N. Curren et al.: A High Efficiency, Low Power Ka-Band TWTA for Cassini, Prepared for the 1994 IEEE IEDM, San Francisco, CA, pp. 783–786, December 11–14, 1994.
14. Personal communication with Ron LeBorgne of Hughes Aircraft Co., Electron Dynamics Division.
15. J. W. Gewartowski and H. A. Watson: Principles of Electron Tubes. D. Van Nostrand Company, Inc., p. 357, 1965.
16. S. Ramo, J. R. Whinnery and T. Van Duzen: Fields and Waves in Communications Electronics, 2nd ed. John Wiley and Sons, New York, p. 238, 1984.
17. O. P. Ghandi: Microwave Engineering and Applications. Pergamon Press, Elmsford, New York, 1981.
18. A. S. Gilmour, Jr., M. R. Gillette and J-T. Chen: Theoretical and Experimental TWT Helix Loss Determination, *IEEE Trans. on Electron Devices,* vol. 26, no. 10, pp. 1581–1588, October 1979.
19. A. S. Gilmour, Jr.: Principles of Traveling-Wave Tubes, Artech House, Boston, MA, p. 327, 1994.
20. S. Alterovitz et al.: Characterization of Commercial APBN, NASA Technical Paper in preparation.
21. J. C. Slater: Microwave Electronics. Van Nostrand, New York, 1950.

APPENDIX A—CALCULATING NTH SPACE HARMONIC ELECTRIC FIELD AMPLITUDE

The total axial electric field on the axis can be represented in terms of a Fourier series,

$$E_{ztot}(z) = \sum_{\infty}^{\infty} a_n \cos(\beta_n z) + b_n \sin(\beta_n z) \tag{A1}$$

with

$$a_n = \frac{2}{P} \int_{-\frac{P}{2}}^{\frac{P}{2}} E_{ztot}(z) \cos(\beta_n z) dz \tag{A2}$$

and

$$b_n = \frac{2}{P} \int_{-\frac{P}{2}}^{\frac{P}{2}} E_{ztot}(z) \sin(\beta_n z) dz \tag{A3}$$

where P is the period of $E_{ztot}(z)$. By defining $z = 0$ at a boundary, $E_{ztot}(z)$ will always be either an even or an odd function with respect to z. If $z = 0$ at an electric wall, $E_{ztot}(z)$ is an even function with $b_n = 0$ and the magnitude of the n^{th} harmonic is obtained from:

$$E_n = \frac{4}{P} \int_{0}^{\frac{P}{2}} E_{ztot}(z) \cos(\beta_n z) dz \tag{A4}$$

If $z = 0$ at a magnetic wall, E_{ztot} is an odd function with $a_n = 0$, and the magnitude of the n^{th} harmonic is obtained from:

$$E_n = \frac{4}{P} \int_{0}^{\frac{P}{2}} E_{ztot}(z) \sin(\beta_n z) dz \tag{A5}$$

APPENDIX B—RELATIONSHIP BETWEEN POWER LOSS FOR TRAVELING AND STANDING WAVES

The electromagnetic energy in the structure per unit length can be expressed as

$$w = \varepsilon \int_{vol} E^2 \, dv \tag{B1}$$

It follows that the total energy associated with a traveling wave can be expressed as

$$W_T = \varepsilon \int_{vol} \sum_{n=-\infty}^{\infty} |A_n \, e^{-j\beta_n z}|^2 \, dv \tag{B2}$$

where A_n is the electric field amplitude of the n^{th} space harmonic. Thus,

$$W_T = \varepsilon \int_{z=0}^{NL} \sum_{n=-\infty}^{\infty} F_n (A_n)^2 \, dz \tag{B3}$$

with

$$F_n = \iint dxdy .$$

Integrating from z=0 to z=NL,

$$W_T = NL\varepsilon \sum_{n=-\infty}^{\infty} F_n (A_n)^2 . \tag{B4}$$

Proceeding in the same manner, the total energy associated with a standing wave can be expressed as

$$W_S = \varepsilon \int_{vol} \sum_{n=-\infty}^{\infty} (2 A_n \cos(\beta_n z))^2 \, dv . \tag{B5}$$

Using the relationship,

$$\int \cos^2(az) dz = \frac{z}{2} + \frac{\sin(2az)}{4a} ,$$

the integral can be evaluated as:

$$W_S = 2NL\varepsilon \sum_{n=-\infty}^{\infty} F_n (A_n)^2 . \tag{B6}$$

Therefore, it can be seen that the energy associated with a traveling wave is half that associated with a standing wave,

$$W_T = \frac{W_S}{2}. \tag{B7}$$

A similar argument can be used to prove that the total power loss associated with a traveling wave, P_{LT}, is half that associated with a standing wave, P_{LS}. The time averaged power loss per unit length can be expressed as

$$P_L = \frac{1}{2\sigma\delta}\int_S H_t \bullet H_t^* \, dS \tag{B8}$$

where σ is the conductivity in S/m, δ is the skin depth in m, and H_t is the magnetic field component tangential to the circuit walls. Because the magnetic fields are proportional to the electric fields by a factor η, the intrinsic impedance of the media, it can be deduced that the magnetic fields associated with a traveling wave and a standing wave will have the same relationship as the electric fields associated with a traveling wave and a standing wave. (The value of the field for a traveling wave, E_n, is half that for a standing wave, E_{nS}). It follows that the evaluation of the power loss associated with a traveling wave and a standing wave will also have the same relationship as the electromagnetic energy calculations shown above. Therefore, it can be determined that,

$$P_{LT} = \frac{P_{LS}}{2}. \tag{B9}$$

REPORT DOCUMENTATION PAGE

Form Approved
OMB No. 0704-0188

1. AGENCY USE ONLY (*Leave blank*)	2. REPORT DATE	3. REPORT TYPE AND DATES COVERED
	March 1997	Final Contractor Report

4. TITLE AND SUBTITLE

Validation of an Accurate Three-Dimensional Helical Slow-Wave Circuit Model

5. FUNDING NUMBERS

WU–632–50–5D
C–NAS3–27600

6. AUTHOR(S)

Carol L. Kory

7. PERFORMING ORGANIZATION NAME(S) AND ADDRESS(ES)

Analex Corporation
3001 Aerospace Parkway
Brook Park, Ohio 44142

8. PERFORMING ORGANIZATION REPORT NUMBER

E–10658

9. SPONSORING/MONITORING AGENCY NAME(S) AND ADDRESS(ES)

National Aeronautics and Space Administration
Lewis Research Center
Cleveland, Ohio 44135–3191

10. SPONSORING/MONITORING AGENCY REPORT NUMBER

NASA CR–4766

11. SUPPLEMENTARY NOTES

This report was submitted as a thesis in partial fulfillment of the requirements for the degree Master of Science in Electrical Engineering to Cleveland State University, Cleveland, Ohio, March 1997. Project Manager, James A. Dayton, Jr., Communications Technology Division, NASA Lewis Research Center, organization code 5600, (216) 433–3515.

12a. DISTRIBUTION/AVAILABILITY STATEMENT

Unclassified - Unlimited
Subject Categories 61 and 31

This publication is available from the NASA Center for AeroSpace Information, (301) 621–0390.

12b. DISTRIBUTION CODE

13. ABSTRACT ***(Maximum 200 words)***

The helical slow-wave circuit embodies a helical coil of rectangular tape supported in a metal barrel by dielectric support rods. Although the helix slow-wave circuit remains the mainstay of the traveling-wave tube (TWT) industry because of its exceptionally wide bandwidth, a full helical circuit, without significant dimensional approximations, has not been successfully modeled until now. Numerous attempts have been made to analyze the helical slow-wave circuit so that the performance could be accurately predicted without actually building it, but because of its complex geometry, many geometrical approximations became necessary rendering the previous models inaccurate. In the course of this research it has been demonstrated that using the simulation code, MAFIA, the helical structure can be modeled with actual tape width and thickness, dielectric support rod geometry and materials. To demonstrate the accuracy of the MAFIA model, the cold-test parameters including dispersion, on-axis interaction impedance and attenuation have been calculated for several helical TWT slow-wave circuits with a variety of support rod geometries including rectangular and T-shaped rods, as well as various support rod materials including isotropic, anisotropic and partially metal coated dielectrics. Compared with experimentally measured results, the agreement is excellent. With the accuracy of the MAFIA helical model validated, the code was used to investigate several conventional geometric approximations in an attempt to obtain the most computationally efficient model. Several simplifications were made to a standard model including replacing the helical tape with filaments, and replacing rectangular support rods with shapes conforming to the cylindrical coordinate system with effective permittivity. The approximate models are compared with the standard model in terms of cold-test characteristics and computational time. The model was also used to determine the sensitivity of various circuit parameters including typical manufacturing dimensional tolerances and support rod permittivity. By varying the circuit parameters of an accurate model using MAFIA, these sensitivities can be computed for manufacturing concerns, and design optimization previous to fabrication, thus eliminating the need for costly experimental iterations. Several variations were made to a standard helical circuit using MAFIA to investigate the effect that variations on helical tape and support rod width, metallized loading height and support rod permittivity, have on TWT cold-test characteristics.

14. SUBJECT TERMS	15. NUMBER OF PAGES
Traveling-wave tube; Helix; Dispersion; Impedance; Attenuation	44
	16. PRICE CODE: A03

17. SECURITY CLASSIFICATION OF REPORT	18. SECURITY CLASSIFICATION OF THIS PAGE	19. SECURITY CLASSIFICATION OF ABSTRACT	20. LIMITATION OF ABSTRACT
Unclassified	Unclassified	Unclassified	